The system Ce–Zn–Si for <33.3 at.% Ce: phase relations, crystal structures and physical properties†

Fainan Failamani,[a] Andriy Grytsiv,[af] Raimund Podloucky,[a] Herwig Michor,[b] Ernst Bauer,[bf] Pavel Brož,[cd] Gerald Giester[e] and Peter Rogl*[af]

Phase equilibria of the system Ce–Zn–Si have been determined for the isothermal section at 600 °C for <33.3 at.% Ce by XRPD and EPMA. This partial section is characterized by the formation of five ternary compounds with homogeneity regions at constant Ce-content and partial substitution of Zn/Si: τ_1-Ce$_7$Zn$_{21}$(Zn$_{1-x}$Si$_x$)$_2$ (unique type; $0.45 \leq x \leq 0.99$), τ_2-Ce(Si$_{1-x}$Zn$_x$)$_2$ (AlB$_2$-type; $0.36 \leq x \leq 0.73$), τ_5-CeZn(Zn$_{1-x}$Si$_x$)$_2$ (CeNiSi$_2$-type; $0.68 \leq x \leq 0.76$), τ_6-CeZn$_2$(Si$_{1-x}$Zn$_x$)$_2$ (ThCr$_2$Si$_2$-type; $0.25 \leq x \leq 0.30$) and τ_7-Ce$_{37}$Zn$_{48}$Si$_{15}$ (structure unknown). Whereas τ_1, τ_2 and τ_5 are stable at 600 and 800 °C, the phases τ_6, τ_7 are unstable at 800 °C. Atom site distribution in the crystal structures of τ_5, τ_6 and {La,Ce}$_7$Zn$_{21}$(Zn$_{1-x}$Ge$_x$)$_2$ have been elucidated from X-ray intensity refinements on single crystals. The small amounts of the stabilizing tetrel element in {La,Ce}$_7$Zn$_{21}$[Zn$_{1-x}$Si(Ge)$_x$]$_2$ suggest a hypothetical binary phase "{La,Ce}$_7$Zn$_{23}$". The stabilizing effect of Ge in Ce$_7$Zn$_{23-x}$Ge$_x$ has been elucidated from density functional theory (DFT) calculations discussing the electronic structure in terms of the density of states (DOS) and defining enthalpies of formation for Ce$_7$Zn$_{23-x}$Ge$_x$ ($x = 0$, 0.5, 2) as well as for several neighbouring binary Ce–Zn phases. A Schultz–Scheil diagram for the solidification behaviour in the (Zn,Si)-rich part of the diagram was constructed from DTA measurements in closed silica crucibles along with partial isothermal sections determined in the temperature range from 400 to 900 °C. The phases τ_5 and τ_6 both form in degenerate ternary peritectic reactions: L + CeSi$_2$,β-Ce$_2$Zn$_{17}$ ⇔ τ_5 at 865 ± 5 °C and L + τ_5,CeZn$_{11}$ ⇔ τ_6 at 695 ± 5 °C, respectively. Magnetic susceptibility, specific heat and resistivity measurements of τ_5-CeZn(Zn$_{1-x}$Si$_x$)$_2$ revealed Kondo lattice behavior with ferromagnetic ordering below $T_C = 4.4$ K, whereas susceptibility and specific heat studies of τ_6-CeZn$_2$(Zn$_{0.28}$Si$_{0.72}$)$_2$ revealed Curie–Weiss paramagnetic behaviour down to 3 K. The effective paramagnetic moments of Ce obtained from Curie–Weiss fits of τ_5 (2.50μ_B) and τ_6 (2.34μ_B) reveal a ground state close to trivalent Ce.

[a] *Institute of Physical Chemistry, University of Vienna, Währingerstraße 42, A-1090 Vienna, Austria. E-mail: fai.failamani@gmail.com; andriy.grytsiv@univie.ac.at; raimund.podloucky@univie.ac.at; peter.franz.rogl@univie.ac.at; Fax: +43 142779524; Tel: +43 1427752456*

[b] *Institute of Solid State Physics, Vienna University of Technology, Wiedner Hauptstraße 8-10, A-1040 Vienna, Austria. E-mail: michor@ifp.tuwien.ac.at; bauer@ifp.tuwien.ac.at; Fax: +43 15880113199; Tel: +43 15880113160*

[c] *Masaryk University, Faculty of Science, Department of Chemistry, Kotlarska 2, Brno 61137, Czech Republic*

[d] *Masaryk University, Central European Institute of Technology, CEITEC, Kamenice 753/5, Brno 62500, Czech Republic. E-mail: broz@chemi.muni.cz; Fax: +420 549492443; Tel: +420 549493299*

[e] *Institute of Mineralogy and Crystallography, University of Vienna, Althanstraße 14, A-1090 Vienna, Austria. E-mail: gerald.giester@univie.ac.at; Fax: +43 14277853235; Tel: +43 1427753235*

[f] *Christian Doppler Laboratory for Thermoelectricity, Vienna University of Technology, Wiedner Hauptstraße 8-10, A-1040 Vienna, Austria*

† Electronic supplementary information (ESI) available. See DOI: 10.1039/c5ra02789f

1. Introduction

Ternary compounds Ce–T–Si (T is one of the late transition metals) have been known for their interesting physical properties, such as heavy fermion and unconventional superconductivity,[1,2] Kondo-behaviour and quantum criticalities,[3] intermediate valency,[4] thermoelectric features,[5] etc. Most ternary Ce–T–Si systems have been explored,[6] except for group 12 elements (Zn, Cd, Hg). The high vapor pressure of these metals complicates sample preparation, and requires careful control of compositions. Therefore conventional preparation methods such as arc melting or induction melting in open crucibles cannot be used. However, a few investigations were already concerned with the Ce–Zn–Si system. Kido *et al.*[7] reported paramagnetism and metallic behavior of REZnSi compounds (RE = Ce, Nd, Sm, Gd, Tb, Ho) in the temperature range of 77–300 K. Recently, phase equilibria for the Ce–Zn–Si system have been derived at 800 °C by Malik *et al.*[8] and revealed the existence of 4 ternary compounds, labeled as τ_1 to τ_4. Whilst

the crystal structures of τ_1 and τ_2 and their La-homologues have been elucidated from single crystal X-ray data, the crystal structures of the other compounds remained unresolved. A recent study of $RE_7Zn_{21}Tt_2$-phases (Tt is a tetrel element) by Nian-Tzu Suen and Bobev,[9] prompted among other rare earth elements (La–Nd) the formation of novel cerium compounds $Ce_7Zn_{21}\{Ge,Sn,Pb\}_2$ crystallizing with the structure type first determined by Malik et al.[8] for $\{La,Ce\}_7Zn_{21}(Zn_{1-x}Si_x)_2$. In their latest publication, they also investigated the single crystals of $\{Ce–Pr\}_7Zn_{21}(Zn_{1-x}Si_x)_2$ and their magnetic properties.[10] Their result, especially on the crystal structure of $Ce_7Zn_{21.95}Si_{1.05}$ confirms the work of Malik et al.[8]

The absence of ternary compounds in the Ce-poor part (<33 at.% Ce) of the isothermal section Ce–Zn–Si seems unusual, particularly ternary compounds with $ThCr_2Si_2$ structure or derivative types are encountered in most Ce–T–Si systems (T is a transition metal from Cr to Cu).[11] Therefore also the possibility of compound formation at lower temperature needs to be explored. Indeed the investigation of the Zn/Si-rich part of the Ce–Zn–Si phase diagram at 800 °C (ref. 8) revealed hints for a ternary compound (labelled as τ_5) with composition close to $Ce(Zn_{1-x}Si_x)_3$; $x \approx 0.5$. Our further attempts to investigate this phase at 700 °C prompted another ternary compound (labelled as τ_6) with composition of $Ce_{20}Zn_{53}Si_{27}$, which is also formed from the melt. An electron count on τ_5-$CeZn_{1.5}Si_{1.5}$, considering the valencies of Ce = +3, Zn = +2 and Si = −4 yields balanced electronic charges suggesting a Zintl behaviour interesting for thermoelectric application.

Therefore this work focuses on the investigation of phase equilibria and crystal structures of τ_5 and τ_6, as well as their mechanism of formation and stability. Furthermore the magnetic ground state of cerium in these compounds was of interest. Particularly the small amount of tetrel elements (Tt) to stabilize $\{La,Ce\}_7Zn_{21}(Zn_{1-x}Tt_x)_2$ was investigated by DFT calculations for Tt=Ge to get insight into the electronic DOS, bonding behavior and ground state energies of hypothetical binary Ce_7Zn_{23} in comparison with ternary $Ce_7Zn_{23-x}Ge_x$ ($x = 0.5, 2$).

2. Experimental methods and density functional theory calculation

Most samples were prepared by mixing and cold pressing proper blends of ball milled powders of $CeSi_x$ master alloys with Zn filings inside an Ar filled glove box. Master alloys $CeSi_x$ were prepared by argon arc melting of Ce and Si pieces on a water-cooled copper hearth with a tungsten electrode, while Zn filings were prepared from purified Zn drops. Samples in the Zn-rich corner were then sealed under vacuum or argon and annealed at 600 °C for 4 to 14 days. Samples with low Si(Ge) content (close to binary Ce–Zn) were prepared in a different way. Ce filings, Zn filings, and Si(Ge) powder were mixed in proper ratio, cold pressed, sealed and then subjected to the same heat treatment. All starting materials had a purity of better than 99.9 mass%.

After heat treatment, samples were quenched by submersing the quartz capsules in cold water and analyzed by X-ray powder diffraction with Ge-monochromated CuKα₁-radiation employing a Guinier–Huber image plate recording system. X-ray powder diffraction analyses were performed via Rietveld refinement using the FULLPROF program.[12] Precise lattice parameters were determined referring to Ge as internal standard ($a_{Ge} = 0.565791$ nm). Special treatments were needed to prepare samples for Electron Probe Microanalysis (EPMA) due to their powder-like consistency. Coarse powders of samples were mixed and cold pressed with fine powders of conductive resin in a small steel die (5–6 mm in diameter) prior to hot compacting them together into a coarse powder/granule of conductive resin. Samples were ground and polished under glycerin in order to avoid oxidation and/or hydrolysis. Microstructures and compositions were examined by light optical microscopy (LOM) and scanning electron microscopy (SEM) and EPMA on a Zeiss Supra 55 VP equipped with an energy dispersive X-ray analysis (EDX) detector operated at 20 kV.

Single crystals of τ_5 and τ_6 were grown from Zn flux. Powders of a multiphase alloy with nominal composition $Ce_{20}Zn_{50}Si_{30}$ were mixed and cold pressed with Zn filings in a weight ratio of 1 : 45 and 1 : 57 for τ_5 and τ_6, respectively. The sample billets were sealed under vacuum in quartz capsules, heated to 800 °C, kept at this temperature for 1 hour, and were then slowly cooled with a rate of 6 °C h⁻¹ to 735 °C and 670 °C for τ_5 and τ_6, respectively. After quenching in cold water, the Zn flux matrix was dissolved in cold diluted HCl. No reaction of the single crystal material with HCl was observed during leaching.

Single crystals of $\{La,Ce\}_7Zn_{21}(Zn_{1-x}Ge_x)_2$ were prepared from cold pressed mixtures of La/Ce filings, Zn filings and Ge powder with nominal composition of $La_{25}Zn_{73}Ge_2$ and $Ce_{25}Zn_{70}Ge_5$, respectively. The Ce-containing pellet was sealed under vacuum into a quartz ampoule, heated to 600 °C with a rate of 60 °C h⁻¹, kept at this temperature for 12 h, further heated to 1050 °C at 600 °C h⁻¹, and then slowly cooled to 800 °C with a rate of 10 °C h⁻¹. A slightly different heat treatment was performed to grow single crystals of $La_7Zn_{21}(Zn_{1-x}Ge_x)_2$ heating the pellet to 600 °C at 60 °C h⁻¹, keeping this temperature for 12 h, followed by further heating to 900 °C at a rate of 600 °C h⁻¹, resting at this temperature for 30 minutes, and then slowly cooling to 800 °C at a rate of 6 °C h⁻¹. Single crystals were then mechanically isolated and selected from the crushed regulus.

Inspections on an AXS D8-GADDS texture goniometer assured high crystal quality, unit cell dimensions and Laue symmetry of the single crystal specimens prior to X-ray intensity data collections at room temperature on a Bruker APEXII diffractometer equipped with a CCD area detector and an Incoatec Microfocus Source IμS (30 W, multilayer mirror, Mo-Kα, $\lambda = 0.071069$ nm). Orientation matrices and unit cell parameters were derived using the Bruker APEXII software suite.[13] No additional absorption corrections were performed because of the rather regular crystal shapes and small dimensions of the investigated specimens. The structures were solved by direct methods (SHELXS-97) and were refined with the SHELXL-97 (ref. 14) program within the Windows version WINGX.[15] Crystal structure data were standardized using program STRUCTURE-TIDY.[16]

In order to investigate the thermal stability of τ_5 and τ_6 and to determine the corresponding ternary reaction isotherms, DTA measurements were performed using a Netzsch STA 409 CD/3/403/5/G apparatus. Due to the high vapor pressure of Zn, measurements were performed in closed thin-walled quartz crucibles. Single-phase material of τ_5 and τ_6 was measured from room temperature to 900 °C with a heating/cooling rate of 5 °C min^{-1}. Isothermal annealing served to confirm the phase fields related to the four-phase reactions observed in DTA: for this purpose two alloys in the Zn rich part with nominal compositions, $Ce_{5.9}Zn_{59.8}Si_{34.3}$ and $Ce_{7.6}Zn_{78.4}Si_{14}$, were prepared from powders of $CeSi_x$ and Zn filings and annealed at 500 °C for 4 days. After first reaction, the alloys were powderized to a grain size below 53 μm inside the glove box and were then cold compacted in a steel die (diameter = 10 mm). The pellets were dry-cut into several pieces and sealed in quartz tubes under about 300 mbar Ar and annealed at 400 °C, 650 °C, 710 °C, 750 °C, 770 °C, 790 °C, 810 °C, 850 °C, 860 °C, 870 °C, 880 °C and 900 °C for 1 day each. Single phase samples of τ_5 and τ_6 were prepared in a similar way. The second annealing temperature was 700 and 600 °C for τ_5 and τ_6, respectively. The furnaces were calibrated with standard thermocouples and Sb (melting point = 631 °C).

Dc magnetic susceptibility measurements were performed with a SQUID magnetometer for τ_5 and τ_6 from 2–300 K with various magnetic fields from 0.006 to 6 T on freely rotating single crystals with a total mass of 0.80 mg (individual crystals with a typical mass of 100 μg) and on sintered polycrystalline samples of about 20 mg. Ac susceptibility measurements were carried out on sintered polycrystalline samples of about 200 mg with a Lakeshore 7000 ac susceptometer applying an ac-field with amplitude of 325 A m^{-1} and a frequency of 100 Hz. Specific heat measurements were performed on a commercial Quantum Design PPMS calorimeter on a sintered τ_6 sample and on τ_5 single crystals. Parts of a sintered sample of τ_5 were also used for resistivity and Seebeck coefficient measurements. Resistivity measurements were performed from 2–300 K in a

home-made equipment using the ac bridge resistance technique, while the high temperature part (300–673 K) was measured simultaneously with the Seebeck coefficient in a ZEM-3 ULVAC.

The density functional theory (DFT) calculations were performed by using the Vienna *ab initio* simulation package (VASP)[17,18] and applying the pseudopotential construction according to the projector-augmented-wave method.[19] For the exchange-correlation functional the generalized gradient approximation according to Perdew *et al.* (PBE)[20] was chosen. The VASP calculations were done with high precision using the predefined/default values as provided by the VASP package. The energy cutoff was chosen at 350 eV. Spin polarized calculations were done assuming ferro/ferrimagnetic ordering. For the **k** space integration the Gaussian smearing method with a value for σ of 0.1 eV was taken. **k** space grids were constructed by the method outlined in ref. 21, namely 11 × 11 × 11 for CeZn; 7 × 5 × 5 for Ce_4Zn_8 ($CeZn_2$); 7 × 3 × 5 for Ce_4Zn_{12} ($CeZn_3$); 3 × 3 × 7 for $Ce_{14}Zn_{46}$ (Ce_7Zn_{23}) and related compounds; 7 × 3 × 2 for Ce_6Zn_{22} (Ce_3Zn_{11}). No additional many-body treatment was made for the localized character of the f-like states of Ce, since the compounds under study are all in a metallic state with f-occupation of ∼1 per Ce atom. PBE is considered to reasonably capture the localization properties in terms of spin-polarization as it does for 3d transition metals. Assuming the experimental structure as starting point for all cases, the atomic positions as well as the unit cell parameters were fully relaxed. The Ge substitution was made according to Table 3 at the experimentally defined M1 sites.

3. Results and discussions

3.1. Binary boundary systems

The Zn–Si system (calculated) and the Ce–Zn system were accepted after Massalski[22] taking also into account a more recent investigation on the low temperature modification of

Table 1 Crystallographic data of ternary solid phases of the system Ce–Zn–Si

Phase temperature range (°C)	Space group, prototype	Lattice parameters (nm)			Comments
		a	b	c	
τ_1-$Ce_7Zn_{21}(Zn_{1-x}Si_x)_2$	*Pbam*, $Ce_7Zn_{21}(Zn_{1-x}Si_x)_2$	1.55722(3)	1.71942(3)	0.44772(1)	$x = 0.28$ SC (ref. 8)
					$0.28 \leq x \leq 0.98$ at 800 °C (ref. 8)
					$0.45 \leq x \leq 0.99$ at 600 °C [this work]
τ_2-$Ce(Si_{1-x}Zn_x)_2$	*P6/mmm*, AlB_2	0.4223	—	0.4238	$x = 0.50$ (ref. 7)
		0.41827(2)	—	0.42747(2)	SC at $x = 0.44$ (ref. 8)
					$0.36 \leq x \leq 0.76$ at 800 °C (ref. 8)
		0.4421(2)	—	0.38960(3)	$x = 0.75$ (ref. 8)
					$0.36 \leq x \leq 0.73$ at 600 °C [this work]
		0.42206(5)	—	0.42334(6)	$x = 0.47$ [this work]
τ_3-$Ce(Zn_xSi_{1-x})$	Unknown	—	—	—	$0.17 \leq x \leq 0.23$ at 800 °C (ref. 8)
τ_4-$Ce_{40}Zn_{37}Si_{23}$	Unknown	—	—	—	At.% (ref. 8)
τ_5-$CeZn(Zn_{1-x}Si_x)_2$ < 865 ± 5 [this work]	*Cmcm*, $CeNiSi_2$	0.42079(1)	1.76522(3)	0.41619(1)	$x = 0.71$ SC [this work]
					$0.68 \leq x \leq 0.76$ at 600 °C [this work]
τ_6-$CeZn_2(Si_{1-x}Zn_x)_2$ < 695 ± 5 [this work]	*I4/mmm*, $ThCr_2Si_2$	0.41757(1)	—	1.05073(2)	$x = 0.30$ SC [this work]
					$0.25 \leq x \leq 0.30$ at 600 °C [this work]
τ_7-$Ce_{37}Zn_{48}Si_{15}$ < 800	Unknown	—	—	—	This work

Table 2 X-ray single crystal data for τ_5-CeZn(Zn$_{1-x}$Si$_x$)$_2$, $x = 0.71$; space group *Cmcm*, no. 63 and for τ_6-CeZn$_2$(Si$_{1-x}$Zn$_x$)$_2$, $x = 0.30$; space group *I4/mmm*, no. 139

Parameter/compound	τ_5-CeZn(Zn$_{1-x}$Si$_x$)$_2$, $x = 0.71$	τ_6-CeZn$_2$(Si$_{1-x}$Zn$_x$)$_2$, $x = 0.30$
Phase composition (EPMA, at.%)	Ce$_{24.9}$Zn$_{39.6}$Si$_{35.5}$	Ce$_{20.1}$Zn$_{51.8}$Si$_{28.1}$
Refinement composition (at.%)	Ce$_{25.0}$Zn$_{39.7}$Si$_{35.3}$	Ce$_{20.0}$Zn$_{52.0}$Si$_{28.0}$
Structure type	CeNiSi$_2$	ThCr$_2$Si$_2$
2θ range (deg)	$4.62 \leq 2\theta \leq 80.32$	$7.76 \leq 2\theta \leq 72.72$
a [nm]	0.42079(1)	0.41757(1)
b [nm]	1.76522(3)	0.41757(1)
c [nm]	0.41619(1)	1.05073(2)
Reflections in refinement	$537 \geq 4\sigma(F_o)$ of 556	$157 \geq 4\sigma(F_o)$ of 157
Mosaicity	0.55	0.48
Number of variables	20	11
$R_{F2} = \sum|F_o^2 - F_c^2|/\sum F_o^2$	0.0203	0.0077
wR_2	0.0402	0.0197
R_{Int}	0.0432	0.0311
GOF	1.349	1.370
Extinction (Zachariasen)	0.0059(3)	0.034(1)
Ce; occ.	4c (0,y,1/4), $y = 0.39888(1)$; 1.00(−)	2a (0,0,0); 1.00(−)
U_{11}; U_{22}; U_{33}; U_{23}; U_{13}; U_{12}	0.0052(1); 0.0073(1); 0.0038(1); 0; 0; 0	0.00567(9); 0.00567(9); 0.0096(1); 0; 0; 0
M1; occ.	4c (0,y,1/4), $y = 0.03338(5)$; 0.26(1) Zn1 + 0.74 Si1	4d (0,1/2,1/4); 1.00(−) Zn1
U_{11}; U_{22}; U_{33}; U_{23}; U_{13}; U_{12}	0.0137(4); 0.0062(4); 0.0050(4); 0; 0; 0	0.0101(1); 0.0101(1); 0.0090(1); 0; 0; 0
M2; occ.	4c (0,y,1/4), $y = 0.16921(5)$; 0.31(1) Zn2 + 0.69 Si2	4e (0,0,z); $z = 0.38507(5)$; 0.30(1) Zn2 + 0.70(1) Si1
U_{11}; U_{22}; U_{33}; U_{23}; U_{13}; U_{12}	0.0087(4); 0.0080(4); 0.0064(4); 0; 0; 0	0.0087(2); 0.0087(2); 0.0090(2); 0; 0; 0
Zn3; occ.	4c (0,y,1/4), $y = 0.74962(3)$; 1.00 Zn3	
U_{11}; U_{22}; U_{33}; U_{23}; U_{13}; U_{12}	0.0099(2); 0.0082(2); 0.0080(2); 0; 0; 0	
Residual electron density; max; min in (electron per nm^3) × 10^3	2.61; −3.04	0.32; −0.81

αCe$_2$Zn$_{17}$ (αCe$_{1-x}$Zn$_{5+2x}$) with TbCu$_7$-type.[23] For the Ce–Si system we rely on the version of Malik *et al.*,[8] which essentially is based on the investigation by Bulanova *et al.*[24] but also includes further phases such as Ce$_2$Si$_{3-x}$ (ref. 25) and the high pressure phases CeSi$_5$ and Ce$_2$Si$_7$.[26] The La–Zn system was taken from the latest experimental investigation by Berche *et al.*[27] with recent data on the crystal structure of LaZn$_4$.[28] Detailed crystallographic data for unary and binary boundary phases are summarized in Table S1 (ESI†), those for ternary compounds are listed in Table 1, respectively.

3.2. Crystal structure of ternary compounds in the Ce–Zn–Si system

3.2.1. Crystal structure of τ_5-CeZn(Zn$_{1-x}$Si$_x$)$_2$, $x = 0.71$. The X-ray diffraction pattern of a suitable flux grown single crystal of τ_5 was fully indexed in orthorhombic symmetry ($a = 0.42079(1)$, $b = 1.76522(3)$, $c = 0.41619(1)$ nm). Analysis of systematic extinctions suggested three possible space group types *Cmcm*, *Cmc2$_1$*, *C2cm* (non-standard setting) and consequently structure solution employing direct methods was attempted in the space group type *Cmcm* of highest symmetry (see Table 2). In order to find mixed Zn/Si sites, refinements were first performed with Ce and Zn only. Two of the three Zn sites (M1, M2) were found to have an unusually high atomic displacement parameter (ADP), indicating partial substitution by Si atoms.

Further refinement with anisotropic ADPs for all atoms converged to $R_F = 0.020$ and residual electron densities smaller than ± 3.04 e$^-$ Å^{-3}. The final formula obtained, CeZn(Zn$_{1-x}$Si$_x$)$_2$

with $x = 0.71$ corresponds to the composition Ce$_{25.0}$Zn$_{39.7}$Si$_{35.3}$ (in at.%), which perfectly fits to the value derived from EPMA (Ce$_{24.9}$Zn$_{39.6}$Si$_{35.5}$). Details on crystal data along with ADPs are summarized in Table 2. A Rietveld X-ray powder diffraction refinement confirms the structure model for τ_5. Furthermore, lattice parameters, crystal symmetry, and Wyckoff positions proved that this compound is isotypic with the structure type of CeNiSi$_2$ (see Fig. 1).

Interatomic distances are given in Table S2 (ESI†). Comparing atom distances with the sum of atomic radii, direct bonding is neither revealed between M1–Zn3 nor for M2–M2. However, stronger bonding is inferred from the distances among M1–M1, M1–M2 and M2–Zn3 atoms, particularly taking into account the Zn/Si random occupancy. At 600 °C the phase τ_5-CeZn(Zn$_{1-x}$Si$_x$)$_2$ exhibits a compositional range, $0.68 \leq x \leq$
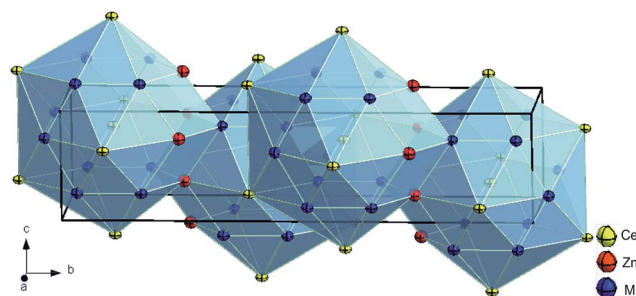
Fig. 1 Crystal structure of τ_5-CeZn(Zn$_{1-x}$Si$_x$)$_2$, $x = 0.71$ showing atoms with anisotropic displacement parameters from X-ray single crystal refinement.

0.76, excluding any stoichiometric composition (for details see Section 3.4).

Compounds with the CeNiSi$_2$ type are known in many Ce–T–Si systems (T = Fe to Cu, Rh, Ir, Pt, and Sn) and exist in both stoichiometric and non-stoichiometric forms.[11] For τ_5-CeZn(Zn$_{1-x}$Si$_x$)$_2$, however, only the non-stoichiometric composition could be found, whereas the Ce–Cu–Si system,[29] which is the closest homologous system, contains two individual phases of same symmetry (isotypic with CeNiSi$_2$), namely CeCu$_{1.6}$Si$_{1.4}$ (≡CeCu(Cu$_{0.6}$Si$_{0.4}$)Si) and stoichiometric CeCuSi$_2$, both separated by a two-phase equilibrium: Ce(Cu$_{1-x}$Si$_{1+x}$)$_2$ (AlB$_2$-type) + CeCu$_2$Si$_2$. It should be noted that the atom preference in the mixed sites in τ_5-CeZn(Zn$_{0.26}$Si$_{0.74}$)(Zn$_{0.31}$Si$_{0.69}$) – where Zn/Si randomly fill two 4c-sites with $y = 0.03338(5)$ and $y = 0.16921(5)$ – differs from non-stoichiometric CeCu(Cu$_{0.6}$Si$_{0.4}$)Si where Cu and Si atoms only share the 4c-site with $y = 0.038$. However, we have to note here that the reliability of the X-ray single crystal study on photographs for CeCu$_{1.6}$Si$_{1.4}$ is low, as R_F was only 17.7%.[30] The discussion on TbFe$_{0.5}$Si$_2$ being a site exchange variant of the CeNiSi$_2$-type has been solved from neutron diffraction data on HoFe$_{0.5}$Si$_2$,[31] which clearly revealed isotypism with the CeNiSi$_2$-type. From the good correspondence of the composition refined from X-ray data with the composition derived from EDX, we can safely conclude that the structure of τ_5-CeZn(Zn$_{1-x}$Si$_x$)$_2$ does not contain any defect sites like HoFe$_{0.5}$Si$_2$.

3.2.2. Crystal structure of τ_6-CeZn$_2$(Si$_{1-x}$Zn$_x$)$_2$, $x = 0.30$. Complete indexation of the X-ray single crystal diffraction data for τ_6 prompted a tetragonal unit cell. The systematic analysis of extinctions suggested $I4$, $I\bar{4}$, $I4/m$, $I422$, $I4mm$, $I\bar{4}2m$, $I\bar{4}m2$ and $I4/mmm$, as possible space group types. Structure solution and refinement employing direct methods in the highest symmetry space group type $I4/mmm$ converged to $R_F = 0.008$ with residual electron densities smaller than ±0.81 e⁻ Å⁻³. Details on crystal data along with ADPs are summarized in Table 2. Unit cell parameters, crystal symmetry, and Wyckoff sites confirm isotypism with the ThCr$_2$Si$_2$ structure type (see Fig. 2).

The final structure formula, CeZn$_2$(Si$_{1-x}$Zn$_x$)$_2$ with $x = 0.30$, reveals one Zn/Si mixed atom site (M = 0.30 Zn2 + 0.70 Si in 4e; 0,0,z), which in many cases provides close contacts among the tetrel elements (dumbbell formation).[32] The formula (Ce$_{20.1}$Zn$_{51.8}$Si$_{28.1}$, in at.%) perfectly fits to the value derived from EDX: Ce$_{20.0}$Zn$_{52.0}$Si$_{28.0}$.

Interatomic distances are given in Table S2 (ESI†). As the M-site is mainly occupied by Si, distances M–M and M–Zn1 are much smaller than distances Zn1–Zn1. Taking into account the random occupancy Zn/Si in the 4e site, the M–M distance is smaller than the sum of radii[33] and is a good indication for dumbbell formation. Comparing the M–M and M–Zn1 distances with those in YbZn$_2$(Si$_{1-x}$Zn$_x$)$_2$; $x = 0.25$,[34] which is hitherto the only far off-stoichiometric REZn$_2$Si$_2$ crystallizing in the ThCr$_2$Si$_2$ type, no significant difference can be found. Consistent with the mixed atom site, τ_6-CeZn$_2$(Si$_{1-x}$Zn$_x$)$_2$ exists

Fig. 3 Micrographs of samples revealing the phase {La,Ce}$_7$Zn$_{21}$(Zn$_{1-x}$Ge$_x$)$_2$ in contact with binary phases from the systems {La,Ce}–Zn.
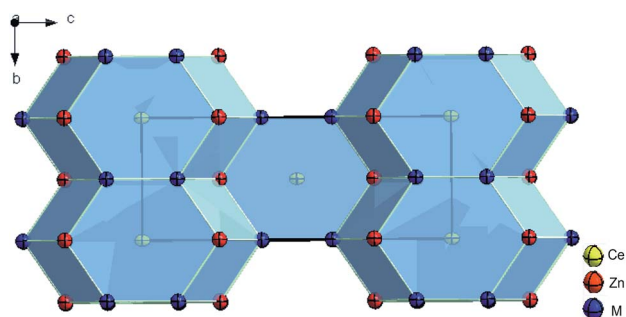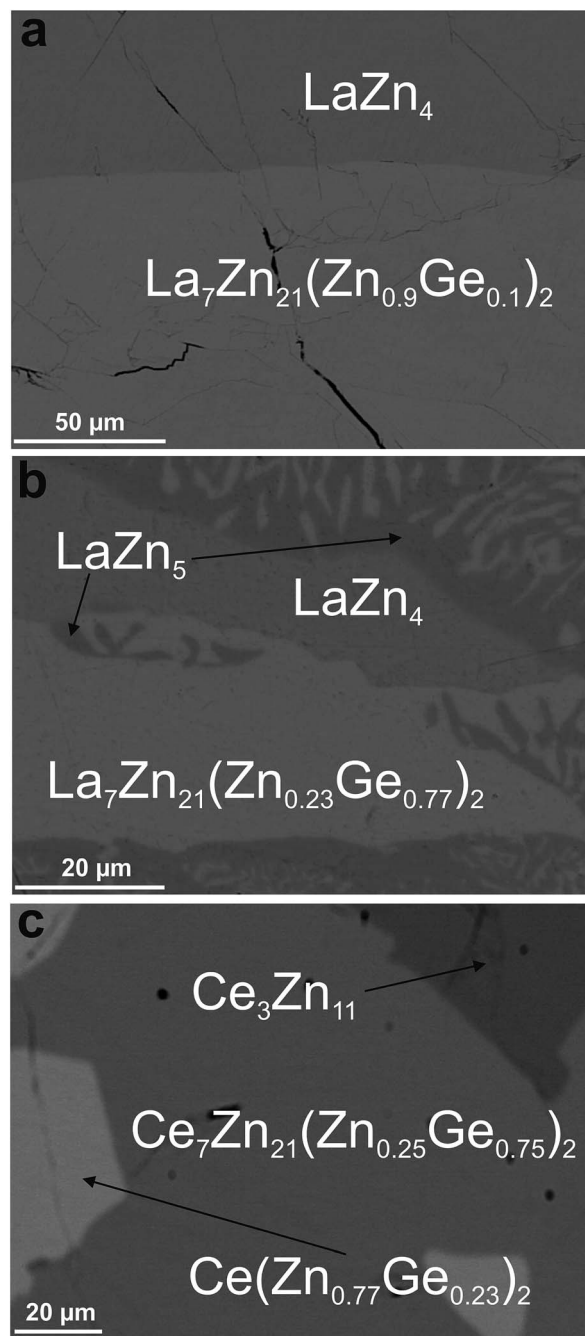

Fig. 2 Crystal structure of τ_6-CeZn$_2$(Si$_{1-x}$Zn$_x$)$_2$, $x = 0.30$ showing atoms with anisotropic displacement parameters from X-ray single crystal refinement.

at 600 °C in a small homogeneity range $0.25 \leq x \leq 0.30$ (for details see Section 3.4). Similar to τ_5 also the phase τ_6 does not include the stoichiometric composition $CeZn_2Si_2$, although first row transition metals mostly form ordered, stoichiometric compounds CeT_2Si_2 (T = Cr to Cu), some with only a small deviation from 1 : 2 : 2 stoichiometry.

3.2.3. Crystal structures of $Ce_7Zn_{21}(Zn_{1-x}Ge_x)_2$ $x = 0.75$ and $La_7Zn_{21}(Zn_{1-x}Ge_x)_2$, $x = 0.10$. In a previous investigation Malik *et al.*[8] found that a surprisingly small amount of only 2 at.% Si was able to stabilize the ternary compound τ_1-Ce_7Zn_{21}-$(Zn_{1-x}Si_x)_2$ ($x = 0.28$, unique structure type) at 800 °C. X-ray single crystal analysis proved $La_7Zn_{21}(Zn_{1-x}Si_x)_2$ ($x = 0.27$) to

Table 3 X-ray single crystal data for $Ce_7Zn_{21}(Zn_{1-x}Ge_x)_2$, $x = 0.75$ and $La_7Zn_{21}(Zn_{1-x}Ge_x)_2$, $x = 0.10$; space group *Pbam*, no. 55. Standardized[a] with program Structure Tidy[16]

Parameter/compound	$Ce_7Zn_{21}(Zn_{1-x}Ge_x)_2$, $x = 0.75$	$La_7Zn_{21}(Zn_{1-x}Ge_x)_2$, $x = 0.10$
Phase composition (EPMA, at.%)	$Ce_{23.2}Zn_{71.9}Ge_{5.0}$	$La_{23.5}Zn_{75.9}Ge_{0.6}$
Refinement composition (at.%)	$Ce_{23.3}Zn_{71.7}Ge_{5.0}$	$La_{23.3}Zn_{76.0}Ge_{0.7}$
Structure type	$Ce_7Zn_{21}(Zn_{1-x}Si_x)_2$	$Ce_7Zn_{21}(Zn_{1-x}Si_x)_2$
2θ range (°)	$4.75 \leq 2\theta \leq 72.58$	$5.19 \leq 2\theta \leq 72.64$
a [nm]	1.55215(2)	1.57043(2)
b [nm]	1.71447(2)	1.73321(3)
c [nm]	0.44836(1)	0.45076(1)
Reflections in refinement	$2706 \geq 4\sigma(F_o)$ of 3103	$2732 \geq 4\sigma(F_o)$ of 3196
Mosaicity	0.45	0.50
Number of variables	94	94
$R_{F2} = \sum|F_o^2 - F_c^2|/\sum F_o^2$	0.0215	0.0330
wR_2	0.0532	0.0609
R_{Int}	0.0147	0.0147
GOF	0.774	1.325
Extinction (Zachariasen)	0.00094(4)	0.00028(3)
RE1 in 4h $(x,y,1/2)$; occ.	$x = 0.16459(2)$; $y = 0.04538(1)$; 1.00(−)	$x = 0.16342(2)$; $y = 0.04474(2)$; 1.00(−)
U_{11}; U_{22}; U_{33}; $U_{23} = U_{13} = 0$; U_{12}	0.0093(1); 0.0094(1); 0.0076(1); −0.0004(1)	0.0099(1); 0.0084(2); 0.0067(1); −0.0003(1)
RE2 in 4g $(x,y,0)$; occ.	$x = 0.16580(2)$; $y = 0.31940(1)$; 1.00(−)	$x = 0.16739(2)$; $y = 0.31848(2)$; 1.00(−)
U_{11}; U_{22}; U_{33}; $U_{23} = U_{13} = 0$; U_{12}	0.0086(1); 0.0087(1); 0.0076(1); −0.00002(7)	0.0096(1); 0.0091(2); 0.0072(1); −0.0005(1)
RE3 in 4g $(x,y,0)$; occ.	$x = 0.41826(2)$; $y = 0.24008(3)$; 1.00(−)	$x = 0.41760(2)$; $y = 0.24148(3)$; 1.00(−)
U_{11}; U_{22}; U_{33}; $U_{23} = U_{13} = 0$; U_{12}	0.0093(1); 0.0195(1); 0.0118(1); −0.0019(1)	0.0104(2); 0.0269(2); 0.0125(2); 0.0037(1)
RE4 in 2c $(0,1/2,0)$; occ.	1.00(−)	1.00(−)
U_{11}; U_{22}; U_{33}; $U_{23} = U_{13} = 0$; U_{12}	0.0103(1); 0.0143(2); 0.0115(2); −0.0030(1)	0.0137(2); 0.0166(3); 0.01304(2); 0.0056(2)
M1 in 4h $(x,y,1/2)$; occ.[b]	$x = 0.02039(3)$; $y = 0.35860(3)$; 0.25 Zn1 + 0.75 Ge1[b]	$x = 0.02098(5)$; $y = 0.35861(4)$; 0.90 Zn1 + 0.10 Ge1[b]
U_{11}; U_{22}; U_{33}; $U_{23} = U_{13} = 0$; U_{12}	0.0091(2); 0.0104(2); 0.0131(2); 0.0001(2)	0.0108(3); 0.0107(4); 0.0165(3); 0.0001(3)
Zn2 in 4h $(x,y,1/2)$; occ.	$x = 0.07520(4)$; $y = 0.21623(3)$; 1.00(−)	$x = 0.07441(5)$; $y = 0.21634(4)$; 1.00(−)
U_{11}; U_{22}; U_{33}; $U_{23} = U_{13} = 0$; U_{12}	0.0143(2); 0.0097(2); 0.0110(2); −0.0008(2)	0.01500(3); 0.0093(3); 0.0102(3); −0.0005(3)
Zn3 in 4h $(x,y,1/2)$; occ.	$x = 0.15224(4)$; $y = 0.44824(3)$; 1.00(−)	$x = 0.15203(5)$; $y = 0.44898(5)$; 1.00(−)
U_{11}; U_{22}; U_{33}; $U_{23} = U_{13} = 0$; U_{12}	0.0128(2); 0.0102(2); 0.0102(2); −0.0019(2)	0.01432(3); 0.01062(4); 0.0096(3); −0.0023(3)
Zn4 in 4h $(x,y,1/2)$; occ.	$x = 0.25707(4)$; $y = 0.21844(3)$; 1.00(−)	$x = 0.25851(5)$; $y = 0.21716(4)$; 1.00(−)
U_{11}; U_{22}; U_{33}; $U_{23} = U_{13} = 0$; U_{12}	0.0134(2); 0.0096(2); 0.0105(2); 0.0005(2)	0.0166(3); 0.0085(3); 0.0093(3); 0.0001(3)
Zn5 in 4h $(x,y,1/2)$; occ.	$x = 0.30414(4)$; $y = 0.35837(3)$; 1.00(−)	$x = 0.30569(5)$; $y = 0.35746(4)$; 1.00(−)
U_{11}; U_{22}; U_{33}; $U_{23} = U_{13} = 0$; U_{12}	0.0128(2); 0.0120(2); 0.0115(2); −0.0032(2)	0.0132(3); 0.0114(4); 0.0107(3); −0.0037(3)
Zn6 in 4h $(x,y,1/2)$; occ.	$x = 0.36349(4)$; $y = 0.09927(3)$; 1.00(−)	$x = 0.36446(5)$; $y = 0.09913(5)$; 1.00(−)
U_{11}; U_{22}; U_{33}; $U_{23} = U_{13} = 0$; U_{12}	0.0105(2); 0.0111(2); 0.0200(3); −0.0005(2)	0.0114(3); 0.0124(4); 0.0223(4); −0.0011(3)
Zn7 in 4h $(x,y,1/2)$; occ.	$x = 0.46584(4)$; $y = 0.40147(4)$; 1.00(−)	$x = 0.46662(5)$; $y = 0.40073(5)$; 1.00(−)
U_{11}; U_{22}; U_{33}; $U_{23} = U_{13} = 0$; U_{12}	0.0103(2); 0.0179(3); 0.0172(3); 0.0029(2)	0.0106(3); 0.0176(4); 0.0178(4); 0.0030(3)
Zn8 in 4g $(x,y,0)$; occ.	$x = 0.07303(4)$; $y = 0.14088(3)$; 1.00(−)	$x = 0.07359(6)$; $y = 0.14124(5)$; 1.00(−)
U_{11}; U_{22}; U_{33}; $U_{23} = U_{13} = 0$; U_{12}	0.0217(3); 0.0141(2); 0.0104(2); 0.0043(2)	0.0260(4); 0.0144(4); 0.0096(3); 0.0046(3)
Zn9 in 4g $(x,y,0)$; occ.	$x = 0.24865(4)$; $y = 0.14674(3)$; 1.00(−)	$x = 0.24920(6)$; $y = 0.14602(5)$; 1.00(−)
U_{11}; U_{22}; U_{33}; $U_{23} = U_{13} = 0$; U_{12}	0.0226 (3); 0.0119(2); 0.0109(2); −0.0050(2)	0.0295(4); 0.0123(4); 0.0099(3); −0.0079(3)
Zn10 in 4g $(x,y,0)$; occ.	$x = 0.29957(4)$; $y = 0.00600(4)$; 1.00(−)	$x = 0.29942(5)$; $y = 0.00570(5)$; 1.00(−)
U_{11}; U_{22}; U_{33}; $U_{23} = U_{13} = 0$; U_{12}	0.0144(3); 0.0197(3); 0.0106(2); 0.0067(2)	0.0166(4); 0.0240(4); 0.0100(3); 0.0099(3)
Zn11 in 4g $(x,y,0)$; occ.	$x = 0.35248(4)$; $y = 0.41919(3)$; 1.00(−)	$x = 0.35252(6)$; $y = 0.41889(5)$; 1.00(−)
U_{11}; U_{22}; U_{33}; $U_{23} = U_{13} = 0$; U_{12}	0.0223(3); 0.0135(2); 0.0100(2); −0.0021(2)	0.0250(4); 0.0134(4); 0.0093(3); −0.0031(3)
Zn12 in 2a $(0,0,0)$; occ.	1.00(−)	1.00(−)
U_{11}; U_{22}; U_{33}; $U_{23} = U_{13} = 0$; U_{12}	0.0147(4); 0.0175(4); 0.0178(4); −0.0010(3)	0.0139(5); 0.0205(6); 0.0172(5); −0.0020(4)
Residual electron density; max; min in (electron per nm³) × 10³	1.59; −1.70	1.71; −2.13

[a] The earlier data sets for single crystal $Ce_7Zn_{21}(Zn_{1-x}Si_x)_2$, $x = 0.28$ (ref. 8) and for isotypic $La_7Zn_{21}(Zn_{1-x}Si_x)_2$, $x = 0.27$,[8] as well as the sets for $\{La–Nd\}_7Zn_{21+x}(Tt)_{2-x}$ (ref. 9 and 10) were not standardized correctly. [b] The occupancy value is fixed after EPMA.

be isotypic.[8] Some controversy exists between the recently reported formation of $Ce_7Zn_{21.3}Ge_{1.7}$ (ref. 9) (isotypic with $Ce_7Zn_{21}(Zn_{1-x}Si_x)_2$) and the investigation of the isothermal section of the homologous system Ce–Zn–Ge at 470 K by Opainich,[35] who did not observe any compound near a composition $Ce_7Zn_{21}Ge_2$. In order to dissolve the controversy it seemed of interest to test the formation of Ge-homologues $\{La,Ce\}_7Zn_{21}(Zn_{1-x}Ge_x)_2$ as well as the extent of their homogeneity regions. Indeed microprobe analyses confirmed that in both systems {La,Ce}–Zn–Ge a phase exists with composition close to the RE-Zn boundary: $La_{23.3}Zn_{71.6}Ge_{5.1}$ and $Ce_{23.3}Zn_{71.7}Ge_{5.0}$ (in at.%; see Fig. 3b and c).

Indexing of the X-ray diffraction data from a suitable single crystal of $Ce_7Zn_{21}(Zn_{1-x}Ge_x)_2$ was complete for an orthorhombic unit cell corresponding to the structure type of $Ce_7Zn_{21}(Zn_{1-x}Si_x)_2$. The structure solution, employing direct methods in space group *Pbam* with the highest symmetry, compatible with the set of systematic extinctions, resulted in the same atom arrangement as for $Ce_7Zn_{21}(Zn_{1-x}Si_x)_2$. Despite the small difference in the X-ray scattering power of Zn and Ge atoms, one mixed Zn/Ge site could unambiguously be identified from the rest of the fully occupied Zn sites. It is the same site as in the parent $Ce_7Zn_{21}(Zn_{1-x}Si_x)_2$ type revealing a slightly smaller ADP and thus requests the presence of an atom with a slightly higher scattering power.

Even though it was possible to refine the occupancy of Zn/Ge (yielding 0.45(5) Zn1 + 0.55(5) Ge1), the ratio Zn/Ge was fixed in accord with the composition obtained from EPMA (0.25 Zn1 + 0.75 Ge1). A final refinement with anisotropic ADPs converged to $R_F = 0.0215$ with a residual electron density less than 1.7 e$^-$ Å^{-3}. Detailed crystal data and atomic displacement parameters are summarized in Table 3. The structure refinement essentially confirmed the data obtained by Suen *et al.*[9] but here for an even lower Ge-content.

Although EPM analyses in the La–Zn–Ge system prompted a phase with composition of $La_{23.3}Zn_{71.6}Ge_{5.1}$ (see Fig. 3b), attempts to grow a single crystal with this Ge content were unsuccessful. However, for lower Ge-contents a suitable single crystal could be obtained (see Fig. 3a). Following the same steps and arguments as for $Ce_7Zn_{21}(Zn_{1-x}Ge_x)_2$, structure solution and refinement of the single crystal data clearly showed isotypism with $Ce_7Zn_{21}(Zn_{1-x}Si_x)_2$. However, due to the low amount of Ge atoms in the unit cell, it was not possible to identify the Zn/Ge mixed site from the rest of the Zn sites. Therefore Ge atoms were placed at the corresponding Si-site as in $Ce_7Zn_{21}(Zn_{1-x}Si_x)_2$ with the occupancy taken from EPMA ($La_{23.3}Zn_{76.0}Ge_{0.7}$ in at.%).

Detailed crystal data and atomic displacement parameters are listed in Table 3. As expected from the isotypism with $Ce_7Zn_{21}(Zn_{1-x}Si_x)_2$, the atomic arrangement in $\{La,Ce\}_7Zn_{21}$-$(Zn_{1-x}Ge_x)_2$ also gives a similar zig-zag chain of distorted $AuCu_3$ and $BaAl_4$ blocks along the *b*-axis (see Fig. 4). This arrangement is similar to Ce_3Zn_{11} with La_3Al_{11}-type, which is the neighbouring phase of $Ce_7Zn_{21}(Zn_{1-x}Ge_x)_2$. Due to the comparable size of Zn and Ge atoms, no significant difference could be found in the interatomic distances between fully occupied Zn and mixed Zn/Ge sites.

The amount of Ge necessary to stabilize the ternary compounds $\{La,Ce\}_7Zn_{21}(Zn_{1-x}Ge_x)_2$ is even less than for isotypic $\{La,Ce\}_7Zn_{21}(Zn_{1-x}Si_x)_2$ and with less than 1 atom percent of Ge infers a rather small degree of thermodynamic instability for the hypothetical binary phases "La_7Zn_{23}" and "Ce_7Zn_{23}".

3.3. Phase stability of $Ce_7Zn_{23-x}Ge_x$

3.3.1. DFT phase stabilities. The enthalpy of formation ΔH_{DFT} at $T = 0$ K was derived from the DFT total energies E_{DFT}^{tot} as obtained from VASP according to:

$$\Delta H_{DFT}(Ce_xZn_{1-x}) = E_{DFT}^{tot}(Ce_xZn_{1-x}) - (xE_{DFT}^{ref}(Ce) + (1-x)E_{DFT}^{ref}(Zn) \quad (1)$$

As reference energies of the pure phases we defined:

$$E_{DFT}^{ref}(Ce) = E_{DFT}^{tot}(Ce) - E_{adj}(Ce), \text{ and}$$
$$E_{DFT}^{ref}(Zn) = E_{DFT}^{tot}(Zn) - E_{adj}(Zn) \quad (2)$$

The DFT energies for the pure phases were calculated for solid nonmagnetic α-fcc-Ce and solid hcp-Zn. It was necessary to adjust the reference energies by $E_{adj}(Ce)$ and $E_{adj}(Zn)$ for a direct comparison with the results of the thermodynamic
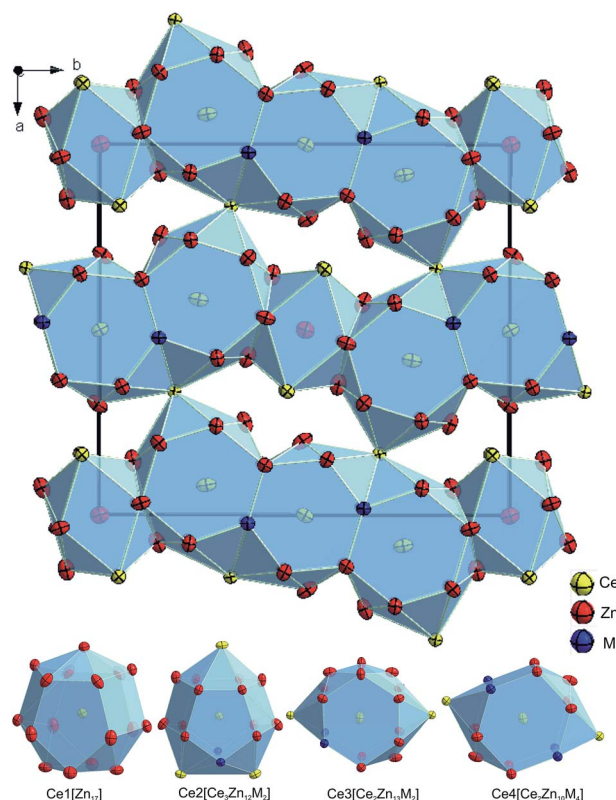

Fig. 4 Crystal structure of $Ce_7Zn_{21}(Zn_{1-x}Ge_x)_2$, $x = 0.75$ projected along the *c*-axis and the coordination polyhedra for the Ce atoms. Atoms are drawn with anisotropic displacement parameters from X-ray single crystal refinement. Please note that (with respect to the previously incorrect standardization of $Ce_7Zn_{21}(Zn_{1-x}Si_x)_2$) the origin of the unit cell is now shifted by (1/2 0 0).

modeling of Wang *et al.*,[36] and experimental work by Chiotti *et al.*[37] and Johnson *et al.*,[38] because of the choice of different reference ground states. Then the values for E_{adj} were extracted by linearly fitting the DFT results (column DFT in Table 4) to the thermodynamic modeling data (column "model") for the four given compounds, and by that $E_{adj}(Ce) = 27.87$ and $E_{adj}(Zn) = 4.38$ kJ mol^{-1} were obtained.

Table 4 summarizes results of the DFT calculations. The DFT derived adjusted enthalpy of formation compares very well with data of the thermodynamic modelling by Wang *et al.*[36] Concerning magnetic properties, as taken from the listed magnetic moments, CeZn does not spin polarize, whereas for the other listed compounds Ce_xZn_{1-x} the magnetic moment per Ce atom decreases with decreasing Ce content, starting with $CeZn_2$ which has the largest local moment per Ce atom of $0.71\mu_B$. For (hypothetical) $Ce_{14}Zn_{46}$ ($x = 0.23$) the local moment is still sizeable amounting to $4.06\mu_B$ for the total magnetic moment of the unit cell. Replacing Zn by Ge in $Ce_{14}Zn_{46-x}Ge_x$ strongly reduces the magnetic moment to less than $0.07\mu_B$ for $x = 1$. The gain in spin-polarization energy is very small being about 0.01 kJ mol^{-1} per Ce atom, which hints at a spin fluctuation system. If $x = 4$ than there is no spin polarization anymore.

The enthalpy of formation for $Ce_x(Ge,Zn)_{1-x}$ compounds was derived similarly to the procedure described above. As a reference, solid Ge was taken in its ground state in the diamond structure. Most noticeable for our study is the stability for the Ge-doped compounds. Even for one Ge atom per formula unit, $Ce_{14}Zn_{45}Ge_1$, ΔH_{DFT} is below the tie-line connecting neighboring Zn-compounds. Here we assume, that in fact the ternary system can be approximately described as a binary one (see Fig. 5). Why Ge stabilizes the compound is analyzed in the following discussing the electronic structure in terms of the density of states (DOS).

3.3.2. DFT phase stabilities for $Ce_7Zn_{23-x}Ge_x$ ($Z = 2$). Panel (a) of Fig. 6 presents the total and atom projected local DOS for $Ce_{14}Zn_{45}Ge_1$. The Fermi energy falls into a sharp uprise of the DOS, which clearly is attributed to the f-states of Ce. At lower energies the DOS is a mixture of Zn and Ce states depending on the energy region. The Ge-DOS features in the range $-2.7 < E <$ -1 eV indicate a more covalent bonding as compared to Zn, which is more pronounced in panel (b) of Fig. 6 showing the local DOS per atom. There the Zn-like DOS is more uniformly spread out in the energy region shown.

The stabilization property of Ge-substitution can be understood by inspecting Fig. 7 showing a reduction of the total DOS at Fermi energy when one Zn is replaced by Ge. This is mainly due to the reduction of the f-like DOS for $Ce_{14}Zn_{45}Ge_1$. The corresponding γ values of the electronic specific heat are 3.43 (DOS at $E_F = 87.3$ states per eV for $Ce_{14}Zn_{46}$) and 3.25 mJ mol^{-1} K^{-2} (DOS at $E_F = 82.7$ states per eV for $Ce_{14}Zn_{45}Ge_1$) indicating poor metals. Analyzing the Ce-f states it turns out that the magnetic moments break down upon Ge substitution, which is responsible for the DOS reduction. The reduction is due to the destruction of the magnetic moment of Ce atoms in the 2c position, because these states are predominant at the Fermi energy for spin polarized $Ce_{14}Zn_{46}$. They carry the largest magnetic moment of all Ce atoms and are therefore the most localized f-states with the largest uprise of all f-DOSes and therefore the largest value at Fermi energy. For $Ce_{14}Zn_{46}$ the local f-moments are 0.27, 0.21, and $0\mu_B$ for the 4-fold coordinated atoms, and $0.74\mu_B$ for the Ce atoms in the 2c position. The breakdown of the magnetic moment upon substitution indicates also a weaker localization and consequently the DOS at Fermi energy is lowered: this leads to the reduction of the total DOS and indicates the thermodynamic stabilization of $Ce_{14}Zn_{45}Ge_1$. Summarizing, the more pronounced covalent bonding between Ce and Ge seems to be the main factor for the stabilization. By substituting 4 Ge atoms the stabilization with respect to the tie-line is considerably enhanced.

3.4. Partial isothermal section at 600 °C for less than 33.3 at.% Ce

The partial isothermal section at 600 °C in the Ce-poor part of the ternary system Ce–Zn–Si was established from EPMA and

Table 4 DFT derived equilibrium heat of formation (DFT) for $T = 0$ K (in kJ mol^{-1}) for $Ce_x(Ge,Zn)_{1-x}$ as a function of Ce concentration x, in comparison to the adjusted DFT values (DFT-adj, see text) and $T = 0$ extrapolation of the thermodynamic modeling (model) of Wang *et al.*[36] For Ce the α-phase was taken as reference. Local magnetic moment per Ce-atom m_{loc} (in μ_B) and the equilibrium volume per atom V_0 (in Å^3) are also given

Compound	x_{Ce}	DFT	DFT-adj	Model	m_{loc}	V_0
CeZn	0.50	−17.81	−33.94	−34.04	0	23.72
CeZn$_2$	0.333	−28.16	−40.37	−40.06	0.71	21.22
CeZn$_3$	0.25	−28.00	−38.25	−38.47	0.25	19.23
Ce$_{14}$Zn$_{46}$	0.233	−26.76	−36.62	—	0.29	19.29
Ce$_{14}$Zn$_{42}$Ge$_4$	0.233	−34.16	−43.73	—	0.19	19.16
Ce$_{14}$Zn$_{45}$Ge	0.233	−28.47	−38.33	—	0.08	19.16
Tie-line	0.233	−27.75	−37.61	—		
Ce$_3$Zn$_{11}$	0.214	−27.47	−36.89	−36.88	0.65	18.66
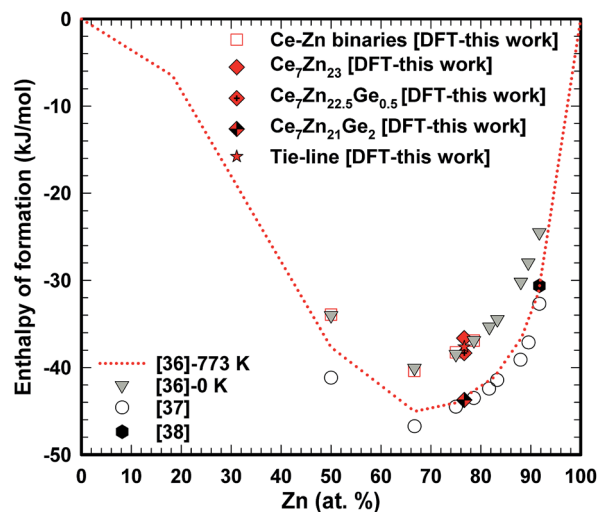
Fig. 5 Comparison between experimental and DFT derived adjusted calculated enthalpies of formation for Ce–Zn binaries and $Ce_7Zn_{23-x}Ge_x$.

X-ray powder diffraction of about 45 alloys (see Fig. 8). Considering the high stability of the phase $Ce(Si_{1-x}Zn_x)_2$ with the αThSi$_2$ type and the relatively slow reaction kinetic at 600 °C (diffusion in cast alloys) the samples were prepared by powder metallurgical techniques *i.e. via* isothermal reaction synthesis starting from compacts of powder/filings in order to ensure establishment of true phase relations at this temperature.
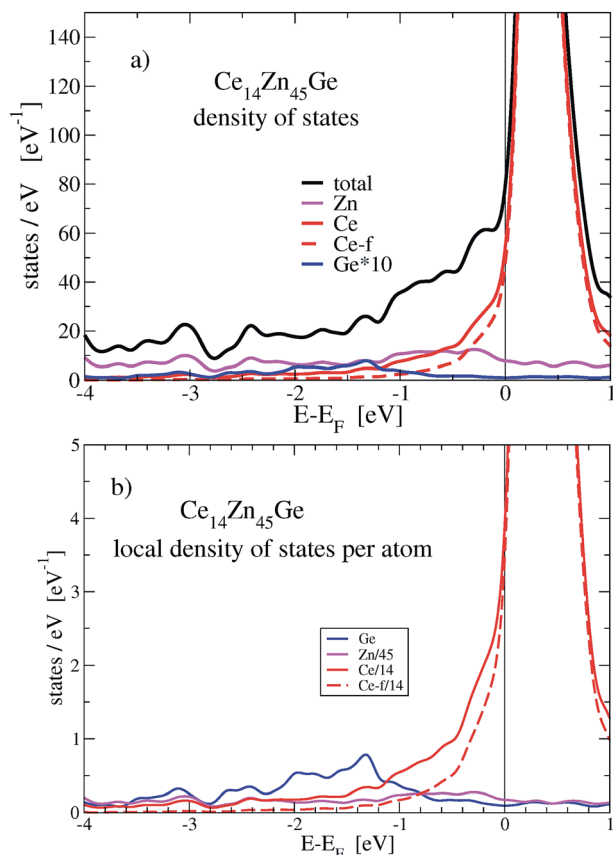

Fig. 6 Panel (a): total and local density of states (DOS) for non spin-polarized $Ce_7Ge_{0.5}Zn_{22.5}$. Panel (b): local DOS per atom. For better visibility, the local DOS for Ge is multiplied by a factor of 10.
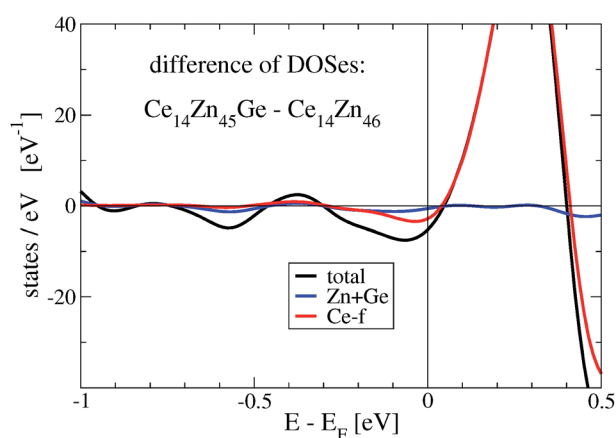
Fig. 7 Differences of total and local density of states, $Ce_7Ge_{0.5}Zn_{22.5}$ minus Ce_7Zn_{23}.

In addition to the ternary compounds τ_1-$Ce_7Zn_{21}(Zn_{1-x}Si_x)_2$, $0.45 \leq x \leq 0.99$ and τ_2-$Ce(Si_{1-x}Zn_x)_2$, $0.36 \leq x \leq 0.73$, both established previously in the 800 °C isothermal section (for details see ref. 8), three new phases, which previously were not encountered at 800 °C,[8] were found to exist at 600 °C: τ_5-$CeZn(Zn_{1-x}Si_x)_2$, τ_6-$CeZn_2(Si_{1-x}Zn_x)_2$, and τ_7-$Ce_{37}Zn_{48}Si_{15}$. Moreover binary $CeZn_{11}$ enters the phase equilibria at 600 °C. Similar to 800 °C, solubility of Si is negligible for all binary compounds $CeZn_x$ with $x > 2$. Extended homogeneity regions were established for τ_1 and τ_2, as well as for τ_5 and τ_6 (Table 1 for details see Table 5). The homogeneity range of τ_1-Ce_7-$Zn_{21}(Zn_{1-x}Si_x)_2$ becomes slightly smaller at 600 °C as compared to 800 °C. The maximum concentration of Si in this phase practically remained the same, while the minimum amount of Si required to stabilize this phase slightly increased from $x = 0.28$ (1.9 at.% Si) at 800 °C to $x = 0.45$ (3.0 at.% Si) at 600 °C. The homogeneity range of τ_1 at 800 °C, studied by combination of XRPD, XRSC, and EPMA contradicts the claim of Hoos *et al.*[10] regarding 3.5 at.% Si as minimum amount of Si in this phase. The three-phase regions involving binary Ce–Zn phases with more than 75 at.% Zn at 600 °C resemble those observed at 800 °C.

Despite all these three-phase equilibrium triangles are narrow, we were able to prepare corresponding samples and to define by EPMA the composition of the equilibrium phases involved. Ternary phases $Ce(Si_{1-x}Zn_x)_2$ (α-ThSi$_2$ type), τ_2, and τ_5 that coexist in three-phase equilibria with binary $CeZn_x$ ($x \geq 5$) crystallized in fine microstructures, which made quantitative analyses by EPMA unreliable. The fine grains could not be agglomerated even with longer annealing time (more than two weeks). Therefore the ternary phases $Ce(Si_{1-x}Zn_x)_2$ with α-ThSi$_2$ type, τ_2, and τ_5, and their composition were determined *via*
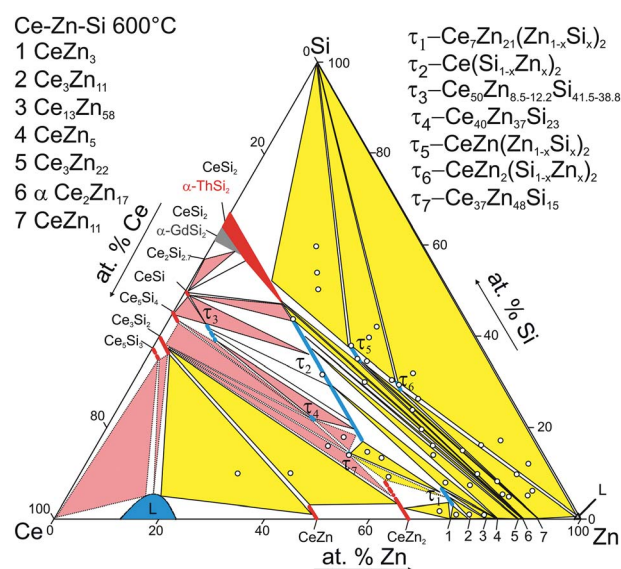

Fig. 8 Partial isothermal section at 600 °C (<33.3 at% Ce). The circles represent nominal compositions of alloys. The pink three phase fields are taken from ref. 8.

Rietveld refinement in combination with the compositional dependence of lattice parameters presented in Fig. 9.

Microstructures of selected three-phase equilibria are given in Fig. 10. Alloys in equilibrium with Si, which were prepared from $CeSi_x$ master alloys containing $CeSi_2$, did not reach complete equilibrium even after re-powderization followed by hot pressing and/or long term annealing. $Ce(Si_{1-x}Zn_x)_2$, $x \leq 0.25$, with α-$ThSi_2$ type was always observed in those alloys. Moreover, long term annealing generally shifted the overall alloy composition due to unavoidable evaporation of Zn,

especially for alloys in the Zn-rich corner. However, equilibrated samples were easily obtained in case binary Ce–Si precursors with Ce content above 40 at.% were used.

Table 5 summarizes data on composition and lattice parameters of all phases coexisting in equilibrium at 600 °C. The only uncertainty concerns the maximal solubility of Si in binary $CeZn_2$. Our various attempts to prepare samples in the corresponding three-phase region $\tau_7 + CeZn_2 + \tau_1$ resulted in non-equilibrium alloys with about 5 at.% Si in the $CeZn_2$-phase. It is noteworthy that the phase triangulation in

Table 5 Three phase equilibria and lattice parameters of alloys annealed at 600 °C

Phase region	Phases	Structure type	EPMA (at.%)			Lattice parameters (nm)		
			Ce	Zn	Si	a	b	c
$\tau_5 + \tau_6 + Si$	τ_5	$CeNiSi_2$	25	36.8	38.2	0.4209(1)	1.7662(5)	0.4177(1)
	τ_6	$ThCr_2Si_2$	20.5	49.8	29.7	0.41881(6)	—	1.0560(4)
	Si	$C_{diamond}$	—	—	—	0.54297(5)	—	—
$CeSi_2 + \tau_5 + Si$	$CeSi_2$	$ThSi_2$	33.0	15.2	51.8	0.42025(3)	—	1.4172(4)
	τ_5	$CeNiSi_2$	24.8	38.1	37.1	0.42046(7)	1.7699(3)	0.41713(3)
	Si	$C_{diamond}$	0.3	0.5	99.2			
$\tau_6 + L(Zn) + Si$	τ_6	$ThCr_2Si_2$	19.9	52.0	28.1	0.41848(3)	—	1.05615(6)
	L(Zn)	Mg	—	—	—			
	Si	$C_{diamond}$	0.0	0.4	99.6	0.54298(4)	—	—
$\tau_6 + L(Zn) + CeZn_{11}$	τ_6	$ThCr_2Si_2$	19.8	51.9	28.3	0.41830(6)	—	1.0558(3)
	L(Zn)	Mg	0.4	99.3	0.3	—	—	—
	$CeZn_{11}$	$BaCd_{11}$	8.6	91.1	0.3	1.0662(1)	—	0.6866(1)
$\tau_5 + CeZn_{11} + Ce_2Zn_{17}$	τ_5	$CeNiSi_2$	—	—	—	0.4210(1)	1.767(1)	0.4165(1)
	$CeZn_{11}$	$BaCd_{11}$	—	—	—	1.0661(1)	—	0.6865(1)
	αCe_2Zn_{17}	$TbCu_7$	10.8	88.8	0.4	0.5253(1)	—	0.4433(1)
$\tau_5 + \tau_6 + CeZn_{11}$	τ_5	$CeNiSi_2$	—	—	—	0.42173(1)	1.75258(2)	0.41738(1)
	τ_6	$ThCr_2Si_2$	—	—	—	0.41872(7)	—	1.0558(1)
	$CeZn_{11}$	$BaCd_{11}$	—	—	—	1.0662(1)	—	0.6868(2)
$\tau_2 + CeSi_2 + Ce_2Zn_{17}$	τ_2	AlB_2	33.3	25.6	41.1^a	0.41365(5)	—	0.42967(5)
	$CeSi_2$	$ThSi_2$	33.3	19.4	47.3^a	0.42029(6)	—	1.4258(4)
	αCe_2Zn_{17}	$TbCu_7$	—	—	—	0.52571(3)	—	0.44397(7)
$\tau_2 + Ce_3Zn_{22} + Ce_2Zn_{17}$	τ_2	AlB_2	33.3	28.8	37.9^a	0.41816(1)	—	0.42592(2)
	Ce_3Zn_{22}	Ce_3Zn_{22}	12.1	87.7	0.2	0.89375(2)	—	2.13790(2)
	αCe_2Zn_{17}	$TbCu_7$	10.7	89.0	0.3	0.52482(6)	—	0.44295(2)
$\tau_2 + CeZn_5 + Ce_3Zn_{22}$	τ_2	AlB_2	33.3	28.9	37.8^a	0.41857(7)	—	0.4260(2)
	$CeZn_5$	$CaCu_5$	16.7	82.8	0.5	—	—	—
	Ce_3Zn_{22}	Ce_3Zn_{22}	12.2	87.4	0.4	0.8937(4)	—	2.138(1)
$\tau_2 + CeZn_5 + \tau_1$	τ_2	AlB_2	33.3	31.3	35.4^a	0.42206(5)	—	0.42334(6)
	$CeZn_5$	$CaCu_5$	—	—	—	0.54236(4)	—	0.42553(5)
	τ_1	Ce_7Zn_{23-x}	22.8	70.6	6.6	—	—	—
$\tau_1 + CeZn_5 + Ce_{13}Zn_{58}$	τ_1	Ce_7Zn_{23-x}	23.1	70.8	6.1	1.4882(2)	1.7238(4)	0.4491(1)
	$CeZn_5$	$CaCu_5$	16.6	83.3	0.1	0.54256(9)	—	0.42542(8)
	$Ce_{13}Zn_{58}$	$Gd_{13}Zn_{58}$	18.0	81.9	0.1	1.4622(2)	—	1.4178(3)
$\tau_1 + Ce_{13}Zn_{58} + Ce_3Zn_{11}$	τ_1	Ce_7Zn_{23-x}	23.1	72.4	4.4	—	—	—
	$Ce_{13}Zn_{58}$	$Gd_{13}Zn_{58}$	17.9	81.9	0.2	—	—	—
	Ce_3Zn_{11}	La_3Al_{11}	21.5	78.3	0.2	—	—	—
$\tau_1 + Ce_3Zn_{11} + CeZn_3$	τ_1	Ce_7Zn_{23-x}	23.1	73.6	3.3	—	—	—
	Ce_3Zn_{11}	La_3Al_{11}	21.4	78.4	0.2	0.4514(1)	0.8879(2)	1.3463(3)
	$CeZn_3$	$CeZn_3$	24.7	75.1	0.2	—	—	—
$\tau_1 + CeZn_2 + CeZn_3$	τ_1	Ce_7Zn_{23-x}	23.3	72.8	4.0	1.5498(4)	1.7107(4)	0.4502(1)
	$CeZn_3$	$CeZn_3$	25.2	74.5	0.3	0.46254(6)	1.0448(5)	0.6641(1)
	$CeZn_2$	$CeCu_2$	32.9	63.8	3.3	0.46417(6)	0.7596(7)	0.7508(1)
$\tau_1 + \tau_7 + \tau_2$	τ_1	Ce_7Zn_{23-x}	23.3	71.1	5.6	—	—	—
	τ_2	AlB_2	33.3	48.4	18.3	0.4388(1)	—	0.39738(7)
	τ_7	Unknown	36.9	48.5	14.6	—	—	—

^{a} The values are calculated from compositional dependence of corresponding lattice parameters (Fig. 9).

this part of the phase diagram at 600 °C is different from that established at 800 °C (ref. 8) and this is essentially due to the formation of τ_7. Thus, two three-phase regions: $Ce(Zn_{1-x}Si_x)_2$(CeCu$_2$-type) + τ_2 + τ_1 and $Ce(Zn_{1-x}Si_x)_2$(CeCu$_2$-type) + τ_2 + τ_4, which were observed at 800 °C are now changed into two three-phase regions: τ_7 + τ_2 + τ_1 and τ_7 + $Ce(Zn_{1-x}Si_x)_2$ (CeCu$_2$-type) + τ_1, possibly due to the peritectoid formation of τ_7 (τ_2 + τ_4 + $Ce(Zn_{1-x}Si_x)_2 \Leftrightarrow \tau_7$), and a U-type reaction (τ_2 + $Ce(Zn_{1-x}Si_x)_2 \Leftrightarrow \tau_1 + \tau_7$) in the temperature interval 600 °C < T < 800 °C.

3.5. Formation of τ_5 and τ_6 and partial Schulz–Scheil diagram

Due to the high melting point of cerium silicides $Ce(Si_{1-x}Zn_x)_2$ and the high vapour pressure of Zn at elevated temperatures, it is difficult to obtain homogeneous cast alloys for the determination of the crystallization behaviour of alloys. On the other hand, the established isothermal section at 600 °C shows that three-phase regions involved in equilibria with binary Ce–Zn compounds are very narrow and our attempts to equilibrate the

samples at higher temperature resulted in a significant change of the overall compositions. Filling the ampoules with argon slightly suppressed the Zn losses, but even in this case samples were heterogeneous, which at first did not allow us to reliably determine the change in phase equilibria via annealing at different temperatures. This shift of the compositions during thermal treatment also hinders the interpretation of DTA. For instance, DTA measurements on single-phase τ_5 and τ_6 resulted in a sequence of several thermal effects that are difficult to reconcile with the phase triangulation. Investigation of the specimens after DTA by SEM/EDX showed that samples became heterogeneous and contained regions with different phases (see Fig. 11). Reliable temperatures for isothermal reactions were only obtained for wide three-phase regions: $CeSi_2$ + τ_5 + (Si), τ_5 + τ_6 + (Si), τ_6 + $CeZn_{11}$ + (Si), $CeZn_{11}$ + (Zn) + (Si). The temperatures of invariant reactions that correspond to these fields were derived as follows: 727 °C, 634 °C, 561 °C and 412 °C, respectively. These four isothermal reaction temperatures were confirmed by DTA from the Zn-rich sample that contains τ_6, (Si), and $CeZn_{11}$ (close to the tie line (Si) + $CeZn_{11}$) (see Fig. 12). After three DTA runs the sample contains additionally τ_5, (Zn), and $CeSi_2$, which suggests incongruent formation of both τ_5 and τ_6.

All invariant reactions determined are summarized in the Scheil reaction scheme in Fig. 13 along with the partial isothermal sections (Fig. 14) at temperatures between the thermal effects established by DTA. Selected microstructures of alloys are presented in Fig. 15 and 16. Comparing the phase equilibria at 500 °C (Fig. 14a) with those observed at 600 °C
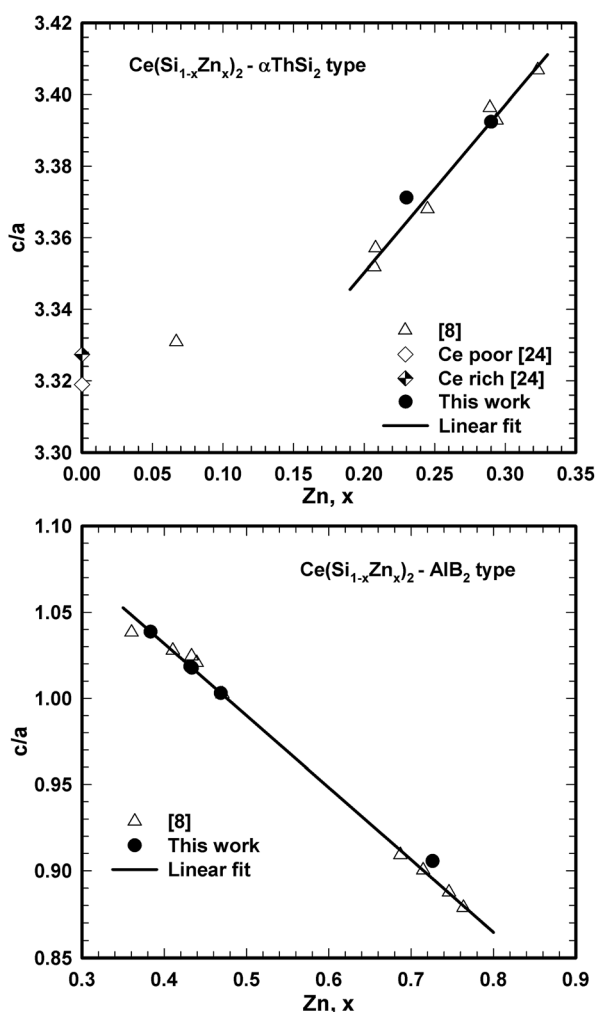

Fig. 9 Compositional dependence of c/a ratio for $Ce(Si_{1-x}Zn_x)_2$ with αThSi$_2$ (left) and AlB$_2$ (right) type.
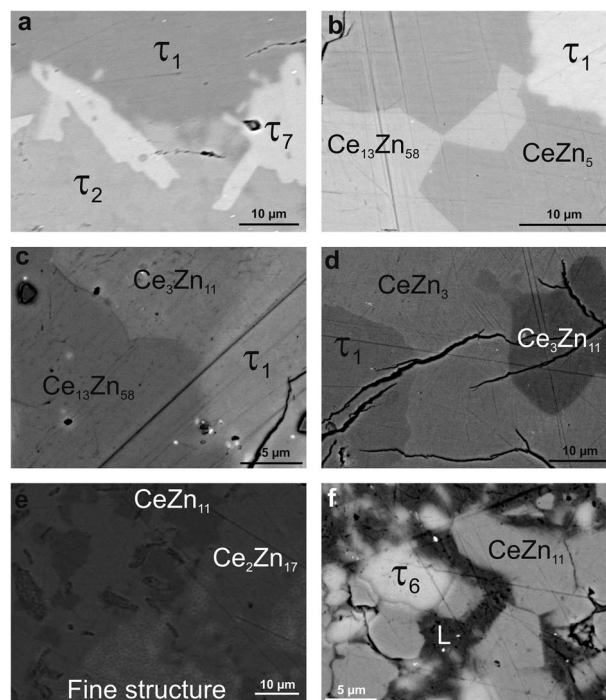

Fig. 10 Selected micrograph of Ce–Zn–Si alloys annealed at 600 °C: (a) $Ce_{32}Zn_{54}Si_{14}$, (b) $Ce_{18}Zn_{81}Si_1$, (c) $Ce_{21}Zn_{78}Si_1$, (d) $Ce_{23}Zn_{76}Si_1$, (e) diffusion couple $Ce_{70}Si_{30}$–Zn (12 hours), and (f) diffusion couple $Ce_{50}Si_{50}$–Zn (12 hours) (nominal composition in at.%).
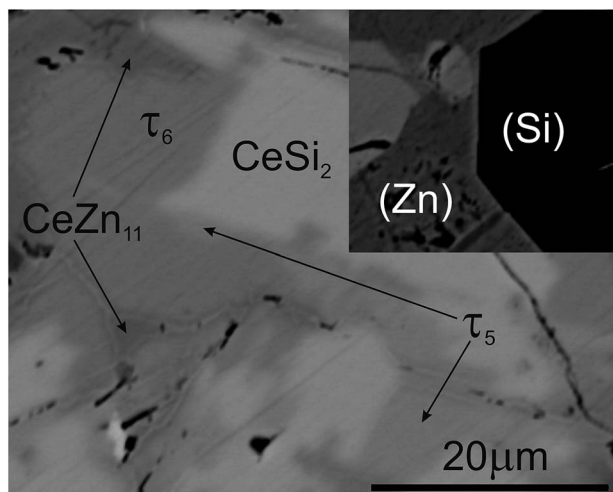
Fig. 11 Micrograph of τ_5 after DTA, showing sequence of crystallization: $CeSi_2$-τ_5-τ_6.

Fig. 13 Scheil diagram for the Zn-rich corner.

(Fig. 14b) we conclude on the existence of a transition type reaction U_1 (561 °C after DTA): L + τ_6 ⇔ $CeZn_{11}$ + (Si).

The characterization of sample $Ce_{5.9}Zn_{59.8}Si_{34.3}$ shows that τ_6 coexists in equilibrium with (Si) and L(Zn) at 600 °C (Fig. 15a), however after annealing at 650 °C τ_6 was not observed in this sample, instead τ_5 enters the equilibrium with L(Zn) and silicon (Fig. 14c and 15b). Such a change of phase equilibria requests another transition type reaction U_2: L + τ_5 ⇔ τ_6 + (Si) to occur between 600 and 650 °C (634° after DTA).

Although τ_6 was observed in the sample $Ce_{7.6}Zn_{78.4}Si_{14}$ annealed at this temperature, τ_6 does not participate in the equilibria at 710 °C (Fig. 14d). It has to be noted that the microstructure of this sample contains four phases (τ_6, τ_5, $CeZn_{11}$, and L(Zn), see Fig. 16b) and one of these phases has to be considered as non-equilibrium phase. Comparing this microstructure with the three-phase structure (τ_5, $CeZn_{11}$ and L(Zn)) obtained for this sample annealed at 750 °C (Fig. 16c) we may safely conclude that τ_6 is the non-equilibrium phase that forms during quenching from 710 °C. On the other hand, the same sample annealed at 690 °C showed only 3 phases (τ_6, $CeZn_{11}$ and L(Zn)). Based on these observations, the invariant reaction for the formation of τ_6 is supposed to occur in the temperature range between 690 and 700 °C (see Fig. 13).
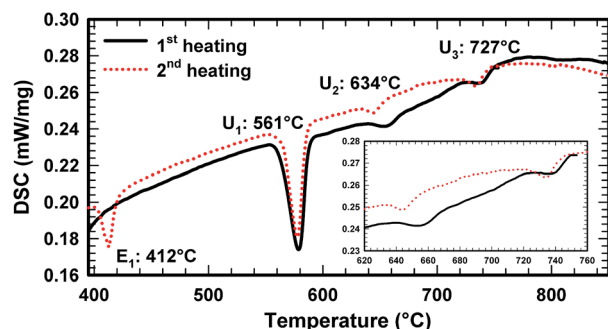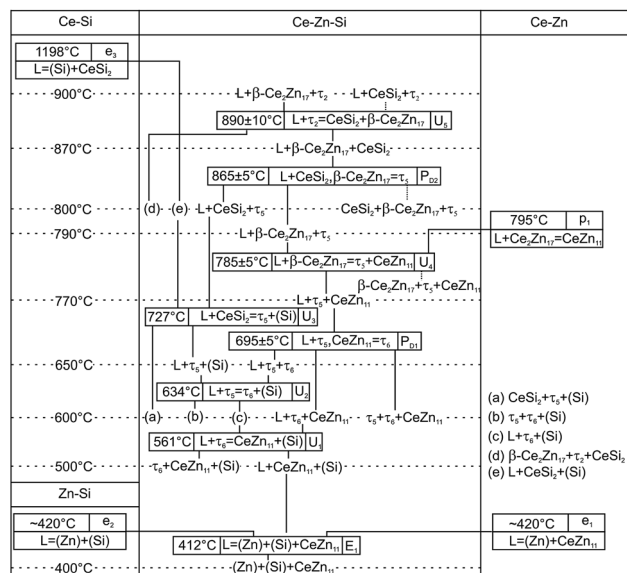

Fig. 12 DTA curve of alloy $Ce_{5.9}Zn_{59.8}Si_{34.3}$.

Three peritectic-type reactions may be responsible for the formation of this phase: (i) L + τ_5 ⇔ τ_6, (ii) L + τ_5 + $CeZn_{11}$ ⇔ τ_6 and (iii) L + τ_5 + (Si) ⇔ τ_6. The latter reaction requests the existence of a three-phase field τ_5 + τ_6 + (Si) at a temperature just below this invariant reaction. However, this three-phase field is not observed at 650 °C (see Fig. 14c), and thus rules out reaction (iii). Rietveld analysis of a sample with composition of $Ce_{24.5}Zn_{37.5}Si_{38.0}$ annealed at 650 °C showed three phases: L(Zn) + τ_5 + τ_6. However due to porosity of the sample it was not possible to reliably analyze the microstructure. Due to a strong degeneracy of the three-phase field L(Zn) + τ_5 + τ_6 (compositions of these phases lie almost on one line; (see Fig. 14c), the two remaining possible invariant reactions (i) and (ii) are almost identical from a thermodynamic point of view.

The existence of a maximum on the solidus in the two-phase field τ_5 + τ_6 would infer a three-phase invariant peritectic L + τ_5 ⇔ τ_6, but due to the difficulties in the interpretation of DTA we cannot provide such evidence. Thus the type of this reaction remains uncertain and is therefore denoted as a degenerated peritectic: L + τ_5, $CeZn_{11}$ ⇔ τ_6 in the temperature range 690 ≤ T ≤ 700 °C (P_{D1}: Fig. 13). The invariant reaction recorded by DTA at 727 °C (Fig. 12) is defined as transition type reaction U_3, L + $CeSi_2$ ⇔ τ_5 + (Si). Confirmation is available from a comparison of the isothermal sections and microstructures of the alloys annealed at 710 (the micrograph is not shown due to its similarity to 650 °C) and 750 °C (Fig. 14d and e and 15b and c). Similar to the narrow three-phase field L(Zn) + τ_5 + τ_6, Rietveld analysis of sample $Ce_{22.7}Zn_{42.9}Si_{34.4}$ annealed at 750 °C revealed three phase constituents: L(Zn), τ_5, and $CeSi_2$ consistent with the three-phase field L(Zn) + τ_5 + $CeSi_2$.

The previously reported isothermal section at 800 °C (ref. 8) suggested that τ_5 is unstable at this temperature and decomposes into $Ce(Si_{1-x}Zn_x)_2$ with α-$ThSi_2$ type, L(Zn), and possibly $CeZn_{11}$ or β-Ce_2Zn_{17}. Indeed DTA runs of sample $Ce_{7.6}Zn_{78.4}Si_{14}$ up to 850 °C gave two signals between 780–790 °C. Surprisingly
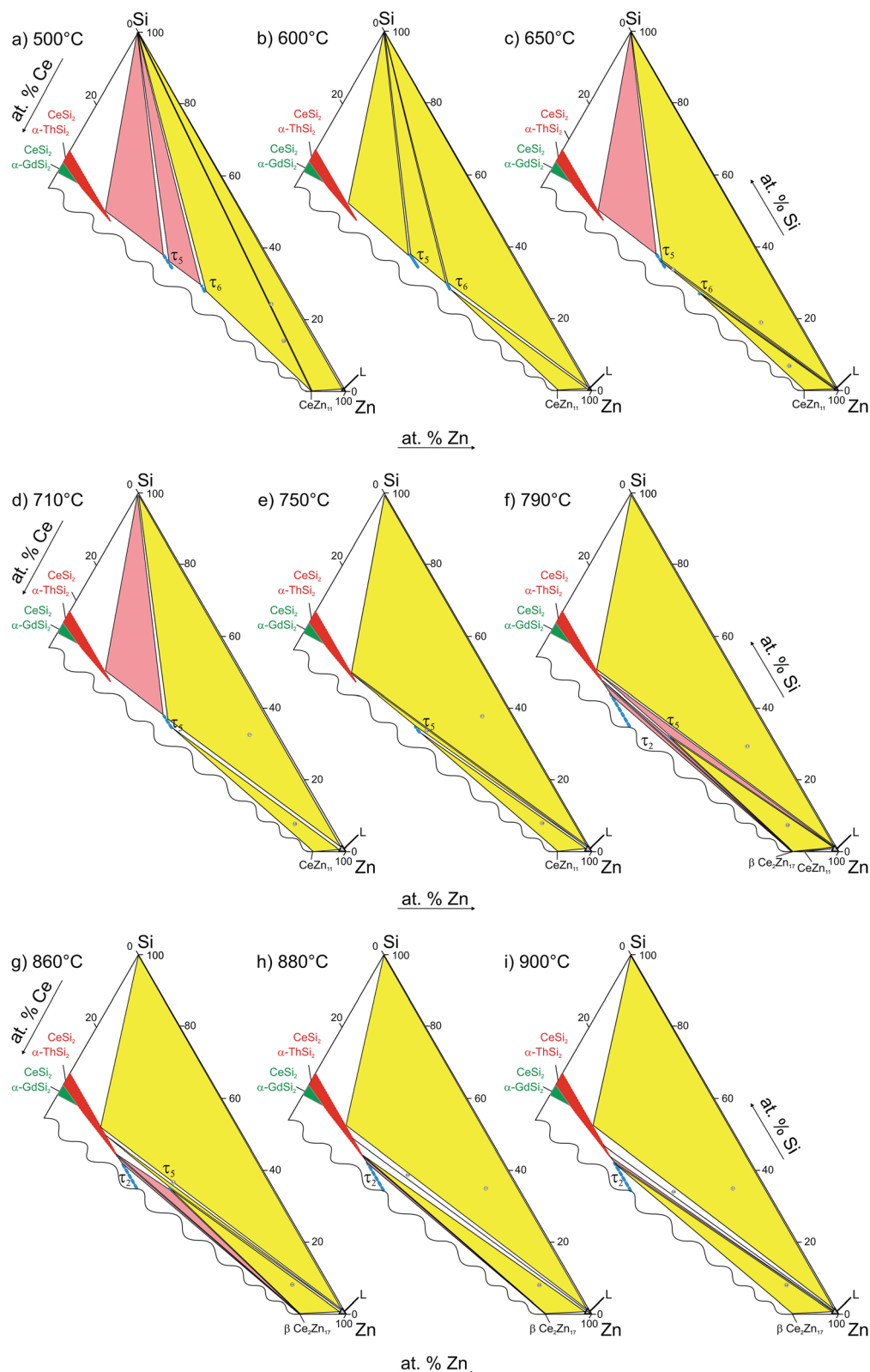
Fig. 14 Partial isothermal sections in the Zn-corner at various temperatures.

EPM analysis of this sample after three DTA runs did not show any trace of $Ce(Si_{1-x}Zn_x)_2$. In order to confirm these observations the remaining pieces of $Ce_{7.6}Zn_{78.4}Si_{14}$ alloys were heat treated at 770, 790, 810, 850, 860, 870, 880 and 900 °C.

Rietveld refinement and EPM analysis clearly showed that τ_5 is still stable up to 850 °C and is in equilibrium with $L(Zn)$ and β-Ce_2Zn_{17}, while at 900 °C it disappears completely yielding a three-phase field $L(Zn) + \beta$-$Ce_2Zn_{17} + \tau_2$. Such a peritectic
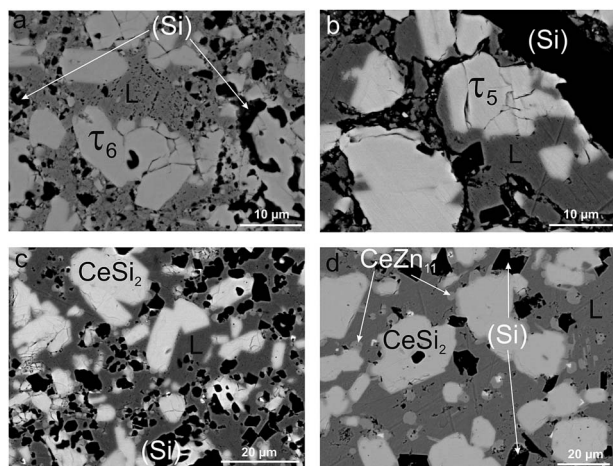
Fig. 15 Microstructure of alloy $Ce_{5.9}Zn_{59.8}Si_{34.3}$ annealed at different temperatures: (a) 600 °C, (b) 650 °C, (c) 750 °C, (d) 900 °C for one day each under argon.

Fig. 17 Isothermal section at 800 °C (modified after ref. 8; see text).

reaction involving τ_2 is not compatible with the existence of the three-phase field $\tau_2 + CeSi_2 + \beta\text{-}Ce_2Zn_{17}$. Careful heat treatment between 850–900 °C followed by XRPD and EPM analysis showed that an alloy annealed at 860 °C gives the same phase constituents as in 850 °C, while at 870 °C $Ce(Si_{1-x}Zn_x)_2$ with α-ThSi$_2$ type is additionally present in this sample. This fact narrows down the decomposition temperature of τ_5 to 865 ± 5 °C, and confirms the participation of $Ce(Si_{1-x}Zn_x)_2$ with α-ThSi$_2$ type in the peritectic formation of τ_5. Taking into consideration

similar arguments, as discussed above for the formation of τ_6, a degenerated invariant reaction of peritectic type P_{D2}: $L + CeSi_2$, $\beta\text{-}Ce_2Zn_{17} \Leftrightarrow \tau_5$ is assigned. The equilibria observed at 900 °C could be explained by a transition type reaction U_5: $L + \tau_2 \Leftrightarrow CeSi_2 + \beta\text{-}Ce_2Zn_{17}$ that occurs at 890 ± 10 °C.

One of the afore-mentioned thermal effects observed between 780–790 °C could be attributed to a transition type reaction U_4: $L + \beta\text{-}Ce_2Zn_{17} \Leftrightarrow \tau_5 + CeZn_{11}$. The phase field $L(Zn) + \tau_5 + CeZn_{11}$ was still observed up to 770 °C, while at 790 °C it changed to $L(Zn) + \tau_5 + \beta\text{-}Ce_2Zn_{17}$. Note that in some samples $CeZn_{11}$ and/or τ_6 were observed as the fourth or fifth phase. Based on the amount and morphology, those phases were considered to be formed during the quenching process.

The stability of τ_5 at 800 °C has been incorporated in the new isothermal section shown in Fig. 17. It supersedes the older version by Malik *et al.*[8] In addition to the three-phase field $L(Zn) + \tau_5 + \beta\text{-}Ce_2Zn_{17}$, two narrow three-phase fields are required to complete the section: $CeSi_2 + \tau_5 + \beta\text{-}Ce_2Zn_{17}$ and $L(Zn) + \tau_5 + CeSi_2$. Note that the three-phase field $L(Zn) + CeSi_2 + (Si)$ is still stable up to 900 °C. Such narrow phase fields are complicated to investigate, and without careful control of the overall sample composition it may earlier have led to a wrong conclusion regarding the stability of τ_5.

The results on the phase equilibria are consistent (i) with the single crystal growth experiments, which reveal a large crystallization field of the αThSi$_2$-type phase $Ce(Si_{1-x}Zn_x)_2$ extending far into the Zn-rich corner (up to 95 at.% Zn), and consequently (ii) with a rather steep liquidus surface in the Zn-rich region, which infers a high degeneracy in the isothermal reactions involving the Zn-rich liquid.

3.6. Physical properties of τ_5-$CeZn(Zn_{1-x}Si_x)_2$ and τ_6-$CeZn_2(Zn_{0.28}Si_{0.72})_2$

Ac magnetic susceptibility measurements on a polycrystalline sample of τ_5 $CeZn(Zn_{0.32}Si_{0.68})_2$ revealed a δ-shape magnetic anomaly near $T_C \sim 5$ K (see Fig. 18) which is indicative of a

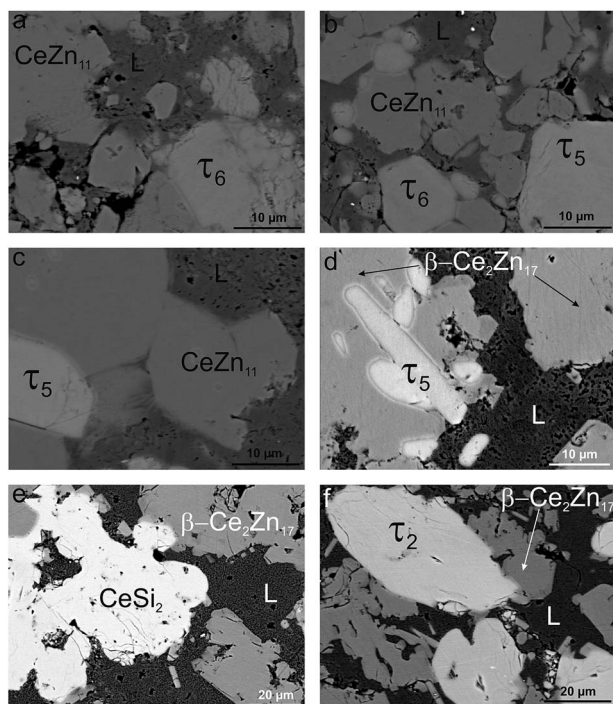**Fig. 16** Microstructure of alloy $Ce_{7.6}Zn_{78.4}Si_{14}$ annealed at different temperatures: (a) 650 °C, (b) 710 °C, (c) 750 °C, (d) 790 °C, (e) 880 °C, and (f) 900 °C for one day each under argon.
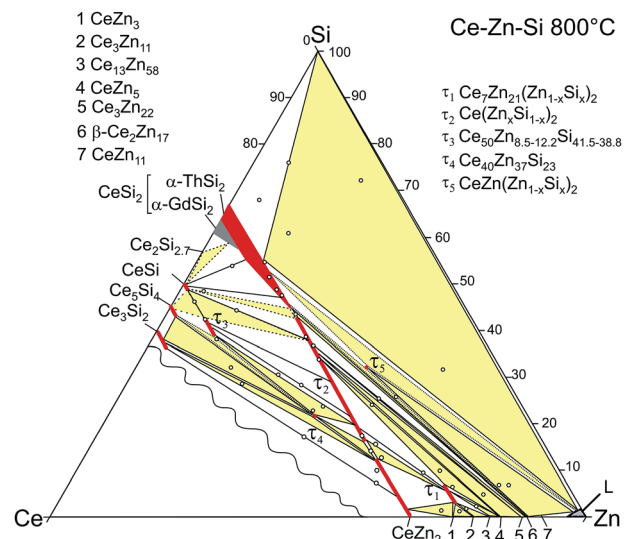
ferromagnetic transition. Accordingly, we performed dc magnetisation and dc susceptibility measurements on a few freely rotating, flux-grown single crystals of τ_5 (with a total mass of 0.8 mg). Field dependent isothermal (see Fig. 19) as well as temperature dependent magnetisation (Fig. 20) measurements confirm ferromagnetic ordering below about 4.4 K with a saturation moment near $1\mu_B$ at 1.9 K and 6 T. The slightly lower T_C of the flux-grown single crystals as compared to the polycrystalline bulk samples relates to slightly different compositions of τ_5 bulk samples as compared to flux grown τ_5 crystals $CeZn(Zn_{0.29}Si_{0.71})_2$.

The ferromagnetic phase transition at $T_C \sim 4.4$ K is corroborated by distinct anomalies of the specific heat and electrical resistivity in Fig. 21 and 22, respectively.

The analysis of the inverse dc magnetic susceptibility in terms of a modified Curie–Weiss fit, $\chi(T) = \chi_0 + C/(T - \Theta_p)$, in Fig. 20 reveals an effective paramagnetic moment of Ce near $2.5\mu_B$ which is close to the effective moment of free Ce^{3+} ($2.54\mu_B$). The negative value of the paramagnetic Curie temperature of -10 K obtained from analysing the data of freely rotating crystals refers to Kondo correlations rather than to a specific type of magnetic coupling (whether antiferro- or ferromagnetic). The relevance of Kondo correlations for τ_5 is further revealed by the temperature dependence of the electrical resistivity in Fig. 22, showing typical Kondo lattice features, and by the specific heat data in Fig. 21. The magnitude of the specific heat anomaly at T_C of τ_5-$CeZn(Zn_{0.29}Si_{0.71})_2$ single crystals is significantly reduced as compared to the value expected from a basic local moment mean-field approach. We thus analyse the temperature dependence and magnitude of the magnetic specific heat contribution in terms of a simple model for a ferromagnetic Kondo lattice system based on the resonant level model by Schotte and Schotte.[39,40] The details of this model calculations are explained *e.g.* in ref. 41.
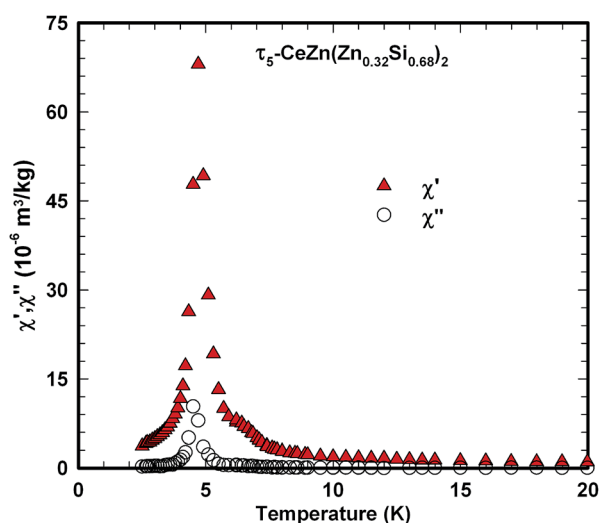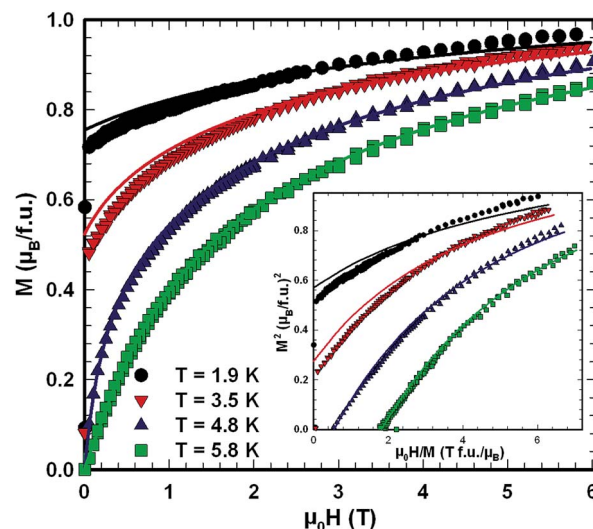

Fig. 19 Isothermal magnetisation measurements of single crystalline τ_5-$CeZn(Zn_{0.29}Si_{0.71})_2$; the inset shows the corresponding Arrott plot, M^2 vs. H/M. The solid lines display a model calculation in terms of the resonant level model by Schotte and Schotte.

The corresponding fit to the experimental data, indicated as solid line in Fig. 21, yields a ferromagnetic exchange coupling $J = 14.6$ K and a Kondo temperature $T_K = 5$ K, thus, suggesting a ferromagnetic Kondo lattice ground state of τ_5-$CeZn(Zn_{0.32}Si_{0.68})_2$. The largest deviation between the applied model and the experimental data is observed right above the ferromagnetic phase transition and relates to short range order and phonon contributions which are not included in the model. Using the same values for J and T_K and an effective Landé factor $g = 2$ to adjust the model for the unknown 4f wave function of the crystal field ground state doublet, we calculated the temperature and field dependent magnetisation displayed as solid lines in Fig. 19. The approximate agreement with the experimental data further supports the validity of a ferromagnetic Kondo model.

Fig. 18 Temperature dependent in-phase and out-of-phase ac susceptibility components, χ' and χ'', measured on polycrystalline τ_5-$CeZn(Zn_{0.32}Si_{0.68})_2$ with a field amplitude of 325 A m^{-1} and frequency of 100 Hz.
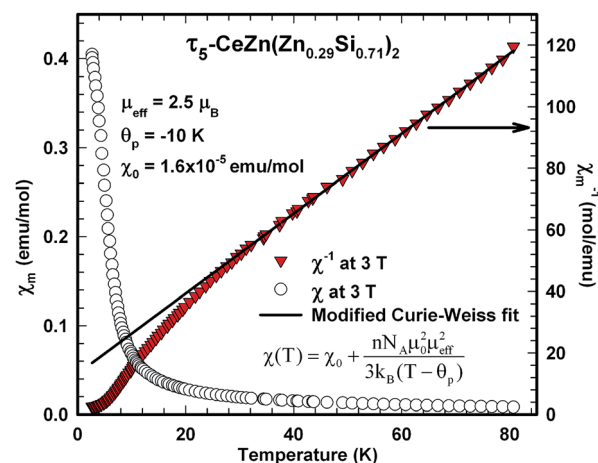

Fig. 20 Temperature dependent dc magnetic susceptibility, $\chi(T)$ at left axis, and inverse magnetic susceptibility, $1/\chi(T)$ at right axis, of freely rotating τ_5-$CeZn(Zn_{0.29}Si_{0.71})_2$ single crystals measured at 3 T; the solid line displays a modified Curie–Weiss fit of the inverse susceptibility.
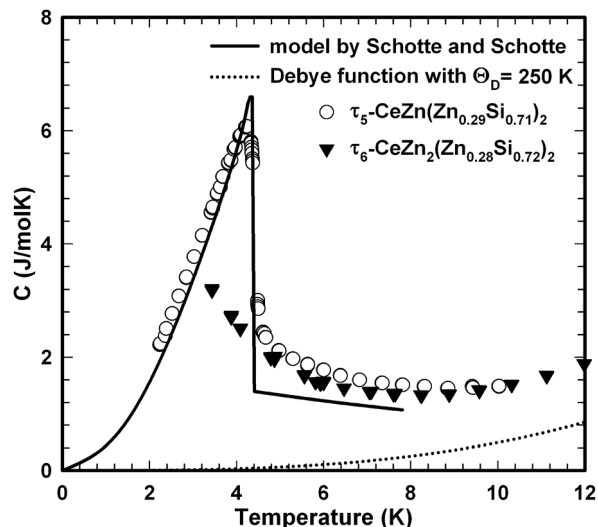
Fig. 21 Temperature dependent specific heat of τ_5-CeZn(Zn$_{0.29}$Si$_{0.71}$)$_2$ single crystals and polycrystalline τ_6-CeZn$_2$(Zn$_{0.28}$Si$_{0.72}$)$_2$; the solid and dotted lines refer to the analysis of τ_5 data in terms of the resonant level model by Schotte and Schotte and a tentative phonon contribution represented by a Debye function, respectively.

The magnetic ground state properties of polycrystalline bulk samples of τ_6 CeZn$_2$(Zn$_{0.28}$Si$_{0.72}$)$_2$ were studied by means of specific heat as well as dc and ac magnetic susceptibility measurements at temperatures down to 3 K. Within the experimental temperature range the τ_6 phase displays a Curie–Weiss type paramagnetic behaviour as demonstrated by the dc magnetic susceptibility depicted in Fig. 23. A modified Curie–Weiss fit of the inverse susceptibility in the temperature interval 80–300 K is indicated as solid line in Fig. 23 and yields a temperature independent Pauli component $\chi_0 = 1.0 \times 10^{-4}$ emu mol^{-1}, a paramagnetic Curie–Weiss temperature $\Theta_p =$

Fig. 22 Temperature dependent electrical resistivity of polycrystalline τ_5-CeZn(Zn$_{0.32}$Si$_{0.68}$)$_2$. Bottom right inset shows the kink at the ordering temperature; top left inset shows the Seebeck coefficient above room temperature.
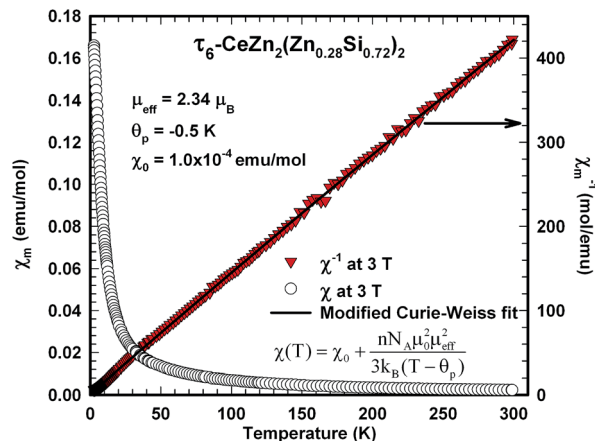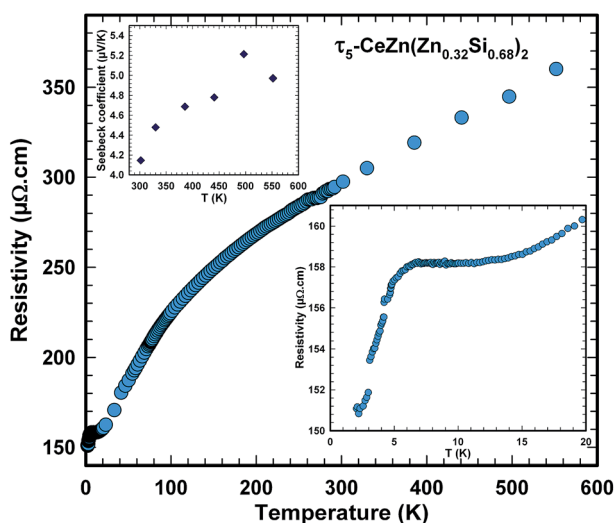

Fig. 23 Temperature dependent dc magnetic susceptibility, $\chi(T)$ at left axis, and inverse magnetic susceptibility, $1/\chi(T)$ at right axis, of polycrystalline τ_6-CeZn$_2$(Zn$_{0.28}$Si$_{0.72}$)$_2$ measured at 3 T; the solid line displays a modified Curie–Weiss fit of the inverse susceptibility.

-0.5 K being indicative for weak antiferromagnetic or very weak Kondo correlations. *Via* the Curie constant of this fit an effective paramagnetic moment $\mu_{eff} = 2.34\mu_B$ is calculated, which is markedly reduced as compared to the Ce^{3+} free ion value (2.54μ_B). The heat capacity data of τ_6 CeZn$_2$(Zn$_{0.28}$Si$_{0.72}$)$_2$ in Fig. 21 display an upturn at lowest temperatures, which may either refer to short range correlations above a magnetic phase transition taking place below 3 K or refer to Kondo correlations with a rather small characteristic energy of the order of one Kelvin.

Consistent with the small Seebeck coefficient (see top left inset in Fig. 22) electrical resistivity of τ_5 indicates metallic type behaviour ruling out any thermoelectrically interesting behaviour.

4. Conclusions

As the Ce–Zn–Si system is an important part of multinary Mg-based Mg–Zn–Mn–RE–(Si) high strength lightweight alloys for automotive applications, we have explored the constitution of the Ce–Zn–Si subsystem and particularly have determined in this work the phase equilibria for the isothermal section at 600 °C in the region with <33.3 at.% Ce. Five ternary compounds (τ_1, τ_2, τ_5 to τ_7) exist at the investigated region at 600 °C. Several four-phase reactions in the Zn rich corner were detected by DTA, including the peritectic decomposition temperatures of τ_5 and τ_6 at 865 ± 5 °C and 695 ± 5 °C, respectively. To provide details on the solidification of Ce-poor alloys, a Schultz–Scheil diagram was constructed from DTA measurements and partial isothermal sections determined at various temperatures. The crystal structures of τ_5 (CeNiSi$_2$-type, *Cmcm*, $a = 0.42079(1)$, $b = 1.76522(3)$, $c = 0.41619(1)$ nm), and τ_6 (ThCr$_2$Si$_2$-type, *I4/mmm*, $a = 0.41757(1)$, $c = 1.05073(2)$ nm) were solved from X-ray single crystal diffraction data. An interesting case was met in the stabilization by extremely small amounts of Ge (less than $\sim$2 atom percent of Ge) of the ternary phases {La,Ce}$_7$Zn$_{21}$-(Zn$_{1-x}$Ge$_x$)$_2$, both isotypic with the structure of

$Ce_7Zn_{21}(Zn_{1-x}Si_x)_2$. DFT calculations elucidated the extent and nature of the stabilizing effect of Ge in $Ce_7Zn_{23-x}Ge_x$ discussing the electronic structure in terms of the density of states (DOS) and determining enthalpies of formation for $Ce_7Zn_{23-x}Ge_x$ ($x = 0, 0.5, 2$) as well as for several neighbouring binary Ce–Zn phases.

Physical property measurements document that neither τ_5 nor τ_6 are near a metal to insulator transition and thus exhibit rather metallic than semiconducting (thermoelectric) behaviour. Magnetic measurements as well as specific heat and electrical resistivity data reveal interesting ferromagnetic Kondo lattice behavior for τ_5-$CeZn(Zn_{1-x}Si_x)_2$ with a Curie temperature $T_C = 4.4$ K, whereas τ_6 displays Curie–Weiss type paramagnetic behavior down to 3 K. The effective paramagnetic moments of Ce obtained from Curie–Weiss fit of τ_5 ($2.50\mu_B$) and τ_6 ($2.34\mu_B$) suggest that the ground state of Ce-ions in these compounds is trivalent or close to 3+.

Acknowledgements

References

1 E. Bauer, G. Hilscher, H. Michor, C. Paul, E. W. Scheidt, A. Gribanov, Y. Seropegin, H. Noël, M. Sigrist and P. Rogl, *Phys. Rev. Lett.*, 2004, **92**, 027003.

2 E. Bauer and P. Rogl, in *Non-Centrosymmetric Superconductors*, ed. E. Bauer and M. Sigrist, Springer, Berlin, Heidelberg, 2012, pp. 3–33.

3 R. Küchler, P. Gegenwart, C. Geibel and F. Steglich, *Sci. Technol. Adv. Mater.*, 2007, **8**, 428.

4 B. Chevalier, P. Rogl, K. Hiebl and J. Etourneau, *J. Solid State Chem.*, 1993, **107**(2), 327–331.

5 A. Amato and J. Sierro, *J. Magn. Magn. Mater.*, 1985, **47–48**, 526–528.

6 P. Rogl, in *Handbook on the Physics and Chemistry of Rare Earths*, ed. K. A. Gschneidner Jr and L. Eyring, Elsevier, 1984, vol. 7, pp. 1–264.

7 H. Kido, T. Hoshikawa, M. Shimada and M. Koizumi, *Phys. Status Solidi A*, 1983, **80**, 601–605.

8 Z. Malik, A. Grytsiv, P. Rogl and G. Giester, *Intermetallics*, 2013, **36**, 118–126.

9 N.-T. Suen and S. Bobev, *Inorg. Chem.*, 2013, **52**, 12731–12740.

10 J. Hoos, N.-T. Suen and S. Bobev, *Acta Crystallogr., Sect. C: Struct. Chem.*, 2014, **70**, 945–948.

11 P. Villars and K. Cenzual, *Pearson's Crystal Data–Crystal Structure Database for Inorganic Compounds, release 2014/15*, ASM International, Materials Park, OH, USA, 2014.

12 J. Rodriguez-Carvajal, *Satellite Meeting on Powder Diffraction of the XV Congress of the IUCR*, Toulouse, France, 1990.

13 *APEXII Software Suite*, Bruker AXS Inc., Madison, Wisconsin, USA, 2005.

14 G. M. Sheldrick, *Acta Crystallogr., Sect. A: Found. Crystallogr.*, 2007, **64**, 112–122.

15 L. J. Farrugia, *J. Appl. Crystallogr.*, 1999, **32**, 837–838.

16 L. M. Gelato and E. Parthé, *J. Appl. Crystallogr.*, 1987, **20**, 139–143.

17 G. Kresse and J. Furthmüller, *Phys. Rev. B: Condens. Matter Mater. Phys.*, 1996, **54**, 11169–11186.

18 G. Kresse and D. Joubert, *Phys. Rev. B: Condens. Matter Mater. Phys.*, 1999, **59**, 1758–1775.

19 P. Blöchl, *Phys. Rev. B: Condens. Matter Mater. Phys.*, 1994, **50**, 17953–17979.

20 J. Perdew, K. Burke and M. Ernzerhof, *Phys. Rev. Lett.*, 1996, **77**, 3865–3868.

21 H. Monkhorst and J. Pack, *Phys. Rev. B: Solid State*, 1976, **13**, 5188–5192.

22 *Pauling File Binary Edition, Version 1.0, Release 2002/1*, ASM international, Materials Park, OH, USA, 2002.

23 Z. Malik, O. Sologub, G. Giester and P. Rogl, *J. Solid State Chem.*, 2011, **184**, 2840–2848.

24 M. V. Bulanova, P. N. Zheltov, K. A. Meleshevich, P. A. Saltykov and G. Effenberg, *J. Alloys Compd.*, 2002, **345**, 110–115.

25 P. Schobinger-Papamantellos and K. H. J. Buschow, *J. Alloys Compd.*, 1993, **198**, 47–50.

26 A. Wosylus, K. Meier, Y. Prots, W. Schnelle, H. Rosner, U. Schwarz and Y. Grin, *Angew. Chem.*, 2010, **122**, 9187–9191.

27 A. Berche, P. Benigni, J. Rogez and M. C. Record, *Thermochim. Acta*, 2011, **523**, 70–78.

28 I. Oshchapovsky, V. Pavlyuk, G. Dmytriv and A. Griffin, *Acta Crystallogr., Sect. C: Cryst. Struct. Commun.*, 2012, **68**, i37–i40.

29 O. I. Bodak, Y. M. Kalychak and E. I. Gladyshevskii, *Izv. Akad. Nauk SSSR, Neorg. Mater.*, 1974, **10**, 450–455.

30 O. I. Bodak, E. I. Gladyshevskii and Y. M. Kalychak, *Tezizy Dokl. Vses. Konf. Kristallokhim. Intermet. Soeden*, 1st edn, 1971.

31 N. M. Norlidah, G. Venturini, B. Malaman and E. Ressouche, *J. Alloys Compd.*, 1998, **265**, 77–80.

32 A. Grytsiv, D. Kaczorowski, A. Leithe-Jasper, P. Rogl, C. Godart, M. Potel and H. Noël, *J. Solid State Chem.*, 2002, **163**, 37–43.

33 L. Pauling and B. Kamb, *Proc. Natl. Acad. Sci. U. S. A.*, 1986, **83**, 3569–3571.

34 A. Grytsiv, A. Leithe-Jasper, H. Flandorfer, P. Rogl, K. Hiebl, C. Godart and T. Velikanova, *J. Alloys Compd.*, 1998, **266**, 7–12.

35 I. M. Opainich, Ph.D. Thesis (in Ukrainian), University of L'viv, 1996.

36 C. P. Wang, X. Chen, X. J. Liu, F. S. Pan and K. Ishida, *J. Alloys Compd.*, 2008, **458**, 166–173.

37 P. Chiotti and J. T. Mason, *Trans. Am. Inst. Min., Metall. Pet. Eng.*, 1965, **233**, 786–795.

38 I. Johnson and R. M. Yonco, *Metall. Trans.*, 1970, **1**, 905–910.

39 K. D. Schotte and U. Schotte, *Phys. Lett. A*, 1975, **55**, 38–40.

40 C. D. Bredl, F. Steglich and K. D. Schotte, *Z. Phys. B: Condens. Matter*, 1978, **29**, 327–340.

41 L. Peyker, C. Gold, E.-W. Scheidt, W. Scherer, J. G. Donath, P. Gegenwart, F. Mayr, T. Unruh, V. Eyert, E. Bauer and H. Michor, *J. Phys.: Condens. Matter*, 2009, **21**, 235604.